Coherent time evolution on a grid of Landau-Zener anticrossings

David A. Harmin

Max-Planck-Institut für Quantenoptik, Hans-Kopfermann-Strasse 1, D-85748 Garching, Germany
and Department of Physics and Astronomy, University of Kentucky, Lexington, Kentucky 40506-0055

A model of the time evolution of two interacting Rydberg manifolds of energy levels subject to a linearly ramped electric field is solved exactly in the Landau-Zener (LZ) approximation. Each manifold's levels are treated as linear in time, parallel, equally spaced, and infinite in number. Their pairwise interactions produce a regular two-dimensional grid of isolated anticrossings. The time development of an initially populated state is then governed by two-level LZ transitions at avoided crossings and adiabatic evolution between them, parametrized by the LZ transition probability D and a dynamical phase unit φ. The resulting probability distributions of levels are given analytically in the form of recursion relations, generating functions, integral representations involving D and φ, and in certain limits by Bessel or Whittaker functions. Level populations are mapped out versus location on the grid for a range of cases. Interference effects lead to two principal types of probability distributions: a braiding adiabatic pattern with revivals for small D and a diabatic pattern for $D \to 1$ in which only certain levels parallel to the initial one are appreciably populated. The sensitivity of the coherent evolution to φ is discussed, along with the relation of this model to others and to selective-field ionization. [S1050-2947(97)06206-9]

PACS number(s): 31.15.−p, 31.70.Hq, 32.60.+i

I. INTRODUCTION

A common problem in atomic physics is the time evolution of a system with many potential-energy curves that cross one another. The dynamics depends on how strongly the states are coupled, the rate at which the curve-crossing region is traversed, the level spacings, and perhaps quite sensitively on coherence effects among the evolving states. In the spectra of Rydberg atoms, n manifolds interact and cross in just this way under the application of increasing dc electric fields. As a case study in the coherent time evolution of interacting sets of states, Rydberg atoms offer several advantages [1,2]. Experimentally, their levels are easy to excite, while external fields can be tuned to control level splittings arbitrarily. On the theoretical side, Rydberg spectra have been widely studied and are often amenable to both simple models and accurate calculations.

Several models [3–7] of interacting manifolds exhibit two generic classes of time evolution patterns, which may be designated roughly as ''adiabatic'' and ''diabatic'' (i.e., nonadiabatic). Different cases can be understood as multilevel or multiple-crossing elaborations on the basic Landau-Zener model [3] of two coupled levels forming an avoided crossing as a function of time. For example, within a single n-manifold of Rydberg-Stark states, the levels fan out nearly linearly from a (near) degeneracy at zero electric field; in nonhydrogenic atoms all levels of the manifold are coupled by the atomic core to form a multilevel anticrossing. When driven by a linearly ramped electric field, there is a strong propensity for an initially populated state to undergo either a purely adiabatic or diabatic transition [4]. In the Demkov-Osherov model [5], on the other hand, an ''interloper'' level varies linearly in time while coupled pairwise to each member of a group of parallel levels. The interloper traverses the group with a survival probability that stems, in effect, from a sequence of nonadiabatic transitions through the group. In

general, the diabatic pattern of the various models is dominated by a single nonadiabatic evolutionary path, even when the level in question is itself a member of a second group of levels crossing the first. This situation is significant only for the most rapid traversals and only if all anticrossing gaps are relatively narrow.

The more common, adiabatic pattern appears as an overall diffusion of population among levels that avoid crossing one another. It might include enhancement of particular states' amplitudes owing to interference. The slower the traversal rate or the larger the anticrossing gaps, the narrower will be the spread of significantly populated levels about the single path that would be found in the adiabatic limit. Such diffusive adiabatic broadening is the principal feature of the time evolution of two groups of interacting levels when coherence effects are ignored [6]. In the present article we investigate the role of coherence in the time evolution of two interacting manifolds of parallel levels, specifically as it affects the adiabatic and diabatic types of evolution.

The aforementioned patterns have been realized experimentally in the many applications of selective-field ionization (SFI) of Rydberg atoms [8]. SFI is used principally to infer Rydberg state populations from ionization signals based on some fairly simple rules [8(a)] for predicting the pathway an initial state will most likely take through the thicket of Rydberg-Stark levels. The identification of general patterns of evolution in such an evolving many-level system, including the degree of diffusion of a state among its neighbors and the appearance of unexpected resonances, is an important step in the reliable interpretation of SFI signals.

In a previous article [6], a model for two interacting manifolds of Rydberg levels was treated in the Landau-Zener (LZ) approximation [3]. Each manifold consists of an infinite set of parallel, equally spaced levels that vary linearly with time t through some controllable parameter, e.g., an external electric field. The manifolds cross and the two sets of states

interact as a function of t. It is further assumed that their coupling is appreciable only in a small neighborhood of each two-level crossing [9] and that this coupling is the same for all pairs of states. The resulting spectrum is a network or grid of pointlike avoided crossings of two bands of linear energy levels. Interference among the states was ignored in order to model the average, gross structure of the probability distributions as a function of time, the field's ramp rate $\dot{F} = dF/dt$, and the coupling strength v. We will refer to Ref. [6] as the PWeb model because only probabilities (not amplitudes) were mixed.

In the present article we keep the LZ approximation but restore interference effects to describe coherent time evolution on the grid; this model is called the AWeb since we properly add state amplitudes. A variation on the AWeb has been investigated by Demkov and co-workers [7], without the assumption of pointlike interactions between pairs of levels. Although Ref. [7] provides the exact energy spectrum of the system and reduces the time-dependent problem to a set of coupled, two-level kicked rotors, the full range of features of the time evolution of two coupled manifolds has not yet been investigated.

To define the AWeb model more explicitly, consider two infinite sets of equally spaced energy levels that vary linearly with time t according to

$$E_m(t) = pt - m\varepsilon, \quad E_{m'}(t) = p't + m'\varepsilon'. \quad (1)$$

This level map is shown in Fig. 1(a) for the general case of unequal spacings and slope magnitudes; Fig. 1(b) shows the case where the level spacings are the same for both manifolds $\varepsilon' = \varepsilon$, while their slopes $p = dE/dt$ are equal and opposite $p' = -p < 0$. Employing the same notation as in Ref. [6], the upward-going levels E_m are numbered $m = 0, 1, 2, \ldots$ from the top down, while the downward-going ones $E_{m'}$ are labeled $m' = 0', 1', 2', \ldots$ from the bottom up. (The indices m and m' should not be confused with the magnetic quantum number m_l.)

In Sec. II we use the two-level LZ result to obtain amplitudes for the up- and down-going levels of the AWeb in the form of recursion relations, generating functions, and integral representations. We present results for a specific case of constructive interference in Sec. III. We discuss the adiabatic and diabatic limits in detail in Secs. IV and V and give analytical results for the up-going amplitudes. Conclusions in Sec. VI touch upon the relation of the AWeb to other models of the time evolution of interacting manifolds and to experiments using selective-field ionization. A simplified derivation of PWeb probabilities is included in the Appendix.

II. AMPLITUDES

To derive an analytical expression for the coherent-state amplitudes, we recast the time evolution on the LZ grid as a two-level problem driven by a generating function. Following the approach of Ref. [6], we label the intersection of levels $E_m(t)$ and $E_{m'}(t)$ as $[m, m']$. This corresponds to time and energy
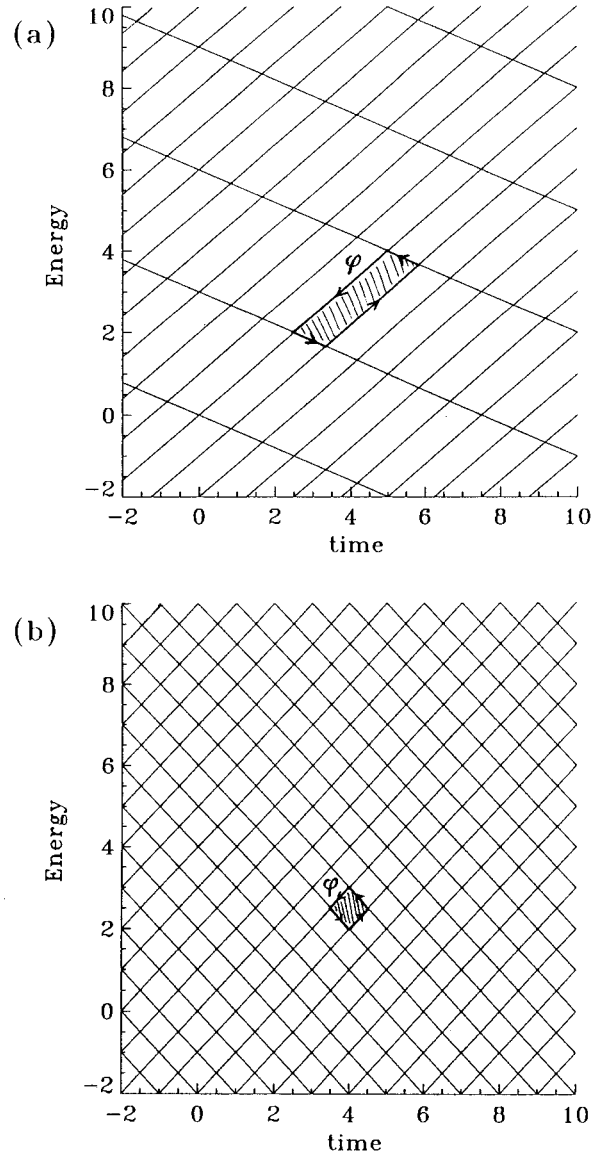
FIG. 1. Generic maps of the energy levels (1) for the AWeb model vs time: (a) skewed map with unequal spacing and asymmetric slopes and (b) symmetric map with equal spacing ($\varepsilon' = \varepsilon$) and opposite slopes ($p' = -p$). Shaded areas shows a unit of action φ [Eq. (8)]; see Ref. [12].

$$t_{mm'} = \frac{m\varepsilon + m'\varepsilon'}{p - p'} \xrightarrow[\substack{\varepsilon' = \varepsilon \\ p' = -p}]{} \frac{\varepsilon}{2p}(m + m'), \quad (2a)$$

$$E_{mm'} = \frac{pm'\varepsilon' + p'm\varepsilon}{p - p'} \xrightarrow[\substack{\varepsilon' = \varepsilon \\ p' = -p}]{} \frac{1}{2}\varepsilon(m' - m), \quad (2b)$$

where the final expressions apply to a symmetric grid. Although neither slope need be negative, we will refer to the states with levels (1) as "up-going" and "down-going" states, respectively. We assume here that only the $m = 0$ level is populated just prior to the intersections at $t = 0$. Given this initial condition, what are the subsequent state populations as a function of time? Specifically, we will de-

rive the amplitudes $\mathcal{A}_{mm'}^{(\uparrow)}(d,\varphi)$ and $\mathcal{A}_{mm'}^{(\downarrow)}(d,\varphi)$ for arriving at intersection $[m,m']$ on the up- and down-going levels $E_m(t)$ and $E_{m'}(t)$, respectively. These will be built up from (i) the nonadiabatic evolution through each avoided crossing and (ii) the adiabatic evolution between avoided crossings.

A. Transitions, dynamical phases, and paths

The basic two-state LZ problem [3] involves two intersecting energy levels m and m' that vary linearly in time, with slopes p and p'. At time t these *diabatic* states have amplitudes $\mathcal{C}_m^{(\uparrow)}(t)$ and $\mathcal{C}_{m'}^{(\downarrow)}(t)$ that are coupled by an interaction $v_{mm'} = \langle m|\hat{H}|m'\rangle$ only at the point of their degeneracy $(t_{mm'}, E_{mm'})$. The probability of beginning in either state $|m\rangle$ or $|m'\rangle$ at $t \ll t_{mm'}$ and making a diabatic (i.e., nondadiabatic) transition to the same state at $t \gg t_{mm'}$ is

$$D \equiv d^2 = \exp\left(-2\pi \frac{|v_{mm'}|^2}{|p-p'|}\right), \quad 0 \leq d \leq 1. \tag{3}$$

The probability of making an adiabatic transition, i.e., switching between up- and down-going levels, is just $A \equiv a^2 = 1-D$ $(0 \leq a \leq 1)$. The amplitudes become mixed by the interaction according to [3]

$$\begin{pmatrix} \mathcal{C}_m^{(\uparrow)}(+\infty) \\ \mathcal{C}_{m'}^{(\downarrow)}(+\infty) \end{pmatrix} = \begin{pmatrix} -d & ae^{i\Phi_S} \\ ae^{-i\Phi_S} & d \end{pmatrix} \begin{pmatrix} \mathcal{C}_m^{(\uparrow)}(-\infty) \\ \mathcal{C}_{m'}^{(\downarrow)}(-\infty) \end{pmatrix}, \tag{4}$$

where the Stokes phase Φ_S is a measure of relative phase accumulation induced by the coupling. In our uniform network of such anticrossings, we assume that every two-state interaction is described by the same values of the parameters d and Φ_S and that the interactions are sufficiently localized in time for the asymptotic mixing (4) to obtain. The phase Φ_S can then be absorbed into all the amplitudes $\mathcal{C}_{m'}^{(\downarrow)}(t)$ and hence ceases to be relevant here [10].

Between these 2×2 interactions the states are assumed to evolve adiabatically. The levels m and m', between their intersection at $[m,m']$ and their arrival at intersections $[m,m'+1]$ and $[m+1,m']$, respectively, acquire the usual dynamical phase factors [11]

$$\begin{pmatrix} \mathcal{C}_m^{(\uparrow)}(t_{m,m'+1}^-) \\ \mathcal{C}_{m'}^{(\downarrow)}(t_{m+1,m'}^-) \end{pmatrix} = \begin{pmatrix} \exp[-iS_{m,m'+1}^{(\uparrow)}] & 0 \\ 0 & \exp[-iS_{m+1,m'}^{(\downarrow)}] \end{pmatrix}$$

$$\times \begin{pmatrix} \mathcal{C}_m^{(\uparrow)}(t_{m,m'}^+) \\ \mathcal{C}_{m'}^{(\downarrow)}(t_{m,m'}^+) \end{pmatrix}, \tag{5}$$

where the actions are

$$S_{m,m'+1}^{(\uparrow)} = \int_{t_{mm'}}^{t_{m,m'+1}} dt\, E_m(t), \tag{6a}$$

$$S_{m+1,m'}^{(\downarrow)} = \int_{t_{mm'}}^{t_{m+1,m'}} dt\, E_{m'}(t) \tag{6b}$$

and $t^{\mp} \equiv \lim_{\epsilon \to 0^+}(t \mp \epsilon)$ indicates the time just before or after t. The *path* from any intersection $[m_1,m_1']$ at time t_1 to a later one, $[m_2,m_2']$ at $t_2 > t_1$, is characterized by a sequence of alternating two-state mixings (4) and adiabatic evolution
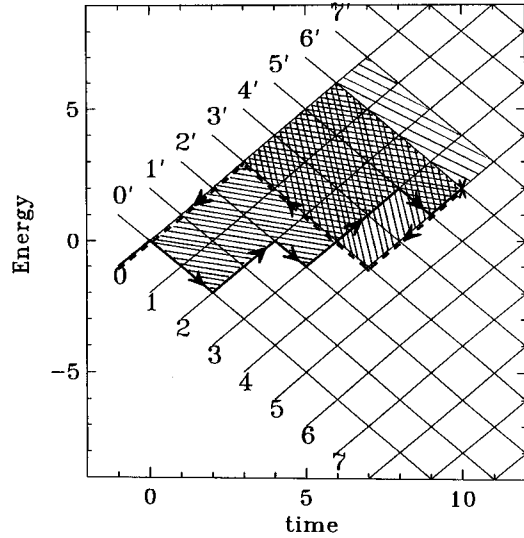
FIG. 2. Two interfering paths from the initial level $m=0$ at intersection $[0,0]$ to up-going level $m=4$ at intersection $[4,6']$ (marked by $\times$). Energy levels (1) are labeled by m and m'. A typical path j (one of 126 possible paths for these end points) is shown by the heavy solid curve; it has area 17φ (shaded) as defined by the action integral in Eq. (11), while its amplitude is $-d^4a^6e^{i17\varphi}$. Another path j' is shown by the heavy dashed curve; it has area 12φ (shaded) and amplitude $-d^8a^2e^{i12\varphi}$. The difference of their actions $\int dt[W_{j'}(t) - W_j(t)] = 5\varphi$ is the net area enclosed by the loop formed by paths j and j', as shown, and enters into the interference term between the two paths in Eq. (12). When either path j or j' continues on to intersection $[4,7']$ its action increases by $m\varphi = 4\varphi$ [Eq. (20)], as shown by light shading.

(5) in the space of all states $|m\rangle$ and $|m'\rangle$. The topology of the network guarantees that only paths for which $m_2 \geq m_1$ and $m_2' \geq m_1'$ have nonzero amplitudes.

During an interval $t_1 \leq t \leq t_2$, any two distinct paths between $[m_1,m_1']$ and $[m_2,m_2']$ will accumulate dynamical phases that interfere as gauged by the phase difference

$$\Delta\Phi = \int_{t_1}^{t_2} dt\, \Delta E(t) \tag{7}$$

for the two paths, as illustrated in Fig. 2. Since Eq. (7) equals the area between the two paths, $\Delta\Phi$ for the grid of levels (1) is always an integral multiple of the unit of action

$$\varphi = \frac{\varepsilon\varepsilon'}{|p-p'|} \xrightarrow[\substack{\varepsilon'=\varepsilon \\ p'=-p}]{} \frac{\varepsilon^2}{2|p|}, \tag{8}$$

which is the area of one parallelogram [12] between pairs of adjacent up- and down-going levels (see Fig. 1). The two parameters D (or d) and φ, representing state-mixing and interference effects, completely characterize the present model, when supplemented by the boundary condition

$$\mathcal{A}_{00'}^{(\uparrow)}(d,\varphi) = \mathcal{C}_0^{(\uparrow)}(t_{00'}^-) = 1, \quad \mathcal{A}_{00'}^{(\downarrow)}(d,\varphi) = \mathcal{C}_{0'}^{(\downarrow)}(t_{00'}^-) = 0 \tag{9}$$

at $t=0$. All other states have zero amplitude at $t=0$ owing to normalization. Although d and φ are regarded here as inde-

pendent parameters, in defining a model of two interacting Rydberg manifolds n and n' they are related through the field ramp rate $\dot{F}$ in $|p-p'|\sim\frac{3}{2}\dot{F}(n^2+n'^2)$. The level spacings at $F>1/3n^5$ are typically $\varepsilon\sim n^{-4}$ and $\varepsilon'\sim n'^{-4}$, while the core-induced couplings can be expressed as $|v_{mm'}|^2 = \tilde{\mu}^2\varepsilon\varepsilon'$, where $\tilde{\mu}$ is an average low-l quantum defect. For a given atomic parameter $\tilde{\mu}$, Eqs. (3) and (8) imply that d and φ are related by

$$d=\exp(-\pi\tilde{\mu}^2\varphi), \quad \varphi\sim(3\dot{F}n^{10})^{-1}. \tag{10}$$

Note, however, that our fundamental assumption of isolated anticrossings requires that $|v_{mm'}|\ll\varepsilon,\varepsilon'$ or $|\tilde{\mu}|\ll1$; thus values in the range $0\leqslant\varphi\leqslant O(1)$ are necessarily tied to the diabatic limit $d\rightarrow1$. On the other hand, the amplitudes will depend not on φ but only on $\varphi(\mathrm{mod}2\pi)$, so the full range of interference effects can be expected for roughly any value of d.

We introduce here a convenient bookkeeping method for accounting for the phases (7). Consider $\mathcal{A}_{mm'}^{(\uparrow)}(d,\varphi)$, the total amplitude for all paths from $[0,0']$ that arrive at $[m,m']$ in the up-going state $|m\rangle$. Each path, numbered j or j', traces out a sequence of diabatic level segments [6], and this sequence defines a continuous energy function $W_j(t)$ describing the path. If $\mathcal{C}_j(t)$ is the amplitude for each path as function of time, then to within an overall phase factor the net amplitude is

$$\mathcal{A}_{mm'}^{(\uparrow)}(d,\varphi)=\sum_{\text{paths }j}|\mathcal{C}_j(t_{mm'}^-)|(-1)^{u_j}$$
$$\times\exp\left(i\int_{t_{00'}}^{t_{mm'}}dt[W_0(t)-W_j(t)]\right) \tag{11}$$

and the total probability is

$$\mathcal{P}_{mm'}^{(\uparrow)}(d,\varphi)=\sum_{j}\sum_{j'}|\mathcal{C}_j(t_{mm'}^-)\mathcal{C}_{j'}(t_{mm'}^-)|(-1)^{u_j+u_{j'}}$$
$$\times\exp\left(i\int_{t_{00'}}^{t_{mm'}}dt[W_{j'}(t)-W_j(t)]\right), \tag{12}$$

where $W_0(t)$ is a reference function defined below. In Eqs. (11) and (12), the sums range over the possible paths [6] $j,j'=1\cdots\binom{m+m'-1}{m}$; $|\mathcal{C}_j(t_{mm'}^-)|$ is a product of $m+m'$ factors of d's and a's; and u_j is the number of up-to-up traversals of avoided crossings along path j [from the amplitudes $-d$ in Eq. (4)]. The action integrals (6) depend on the arbitrary zero of the energy scale to which the levels $E_m(t)$, $E_{m'}(t)$, and $W_j(t)$ are referred. Here all energies are referred to an arbitrary function $W_0(t)$, which preserves all *relative phases* in Eq. (11) and hence all *phase differences* in Eq. (12). We define the action integrals in Eq. (11) to be the difference between $W_j(t)$ and the reference path

$$W_0(t)=\begin{cases}E_0(t), & t_{00'}\leqslant t\leqslant t_{0m'} \\ E_{m'}(t), & t_{0m'}\leqslant t\leqslant t_{mm'}.\end{cases} \tag{13}$$

In a skewed coordinate system with abscissa m and ordinate m', the integral for path j simply equals the area between

that path and the m' axis; see Fig. 2. This area is an integral multiple n_j of the action unit φ [Eq. (8)] with $n_j\geqslant0$:

$$\int_{t_{00'}}^{t_{mm'}}dt[W_0(t)-W_j(t)]=n_j\varphi; \tag{14}$$

therefore, the difference integrals in Eq. (12) are also integral multiples $(n_j-n_{j'})\varphi$, as required. Obviously, the same concepts invoked for the up-going amplitudes in Eqs. (11) and (12) also apply to down-going amplitudes $\mathcal{A}_{mm'}^{(\downarrow)}(d,\varphi)$.

B. Generating functions

Given the constraint (9), successive applications of Eqs. (4) and (5) lead to all state populations at $t\geqslant0$, which we label by the next intersection $[m,m']$ as in Eq. (12):

$$\mathcal{P}_{mm'}^{(\uparrow)}(d,\varphi)=|\mathcal{A}_{mm'}^{(\uparrow)}(d,\varphi)|^2=|\mathcal{C}_m^{(\uparrow)}(t_{mm'}^-)|^2, \tag{15a}$$

$$\mathcal{P}_{mm'}^{(\downarrow)}(d,\varphi)=|\mathcal{A}_{mm'}^{(\downarrow)}(d,\varphi)|^2=|\mathcal{C}_{m'}^{(\downarrow)}(t_{mm'}^-)|^2. \tag{15b}$$

Following Ref. [6], we define the ''generation'' number

$$N=m+m'\geqslant0, \tag{16}$$

which marks the number of avoided crossings that have been encountered between the initial time $t_{00'}^-$, and the approach to $[m,m']$ at time $t_{mm'}^-$. For fixed N we then define the polynomials

$$\mathcal{A}_N^{(\uparrow)}(d,\varphi;\xi,\eta)\equiv\sum_{m=0}^{N}\mathcal{A}_{mm'}^{(\uparrow)}(d,\varphi)\xi^m\eta^{m'}\delta_{m',N-m}, \tag{17a}$$

$$\mathcal{A}_N^{(\downarrow)}(d,\varphi;\xi,\eta)\equiv\sum_{m'=0}^{N}\mathcal{A}_{mm'}^{(\downarrow)}(d,\varphi)\xi^m\eta^{m'}\delta_{m,N-m'}, \tag{17b}$$

where ξ and η are expansion parameters [13] whose powers allow us to keep track of the various states $|m\rangle$ and $|m'\rangle$ at fixed N. With each successive generation, as $N\rightarrow N+1$, a pair of states is first mixed at each $[m,N-m]$ according to Eq. (4) and then each level acquires another dynamical phase factor according to Eq. (5). In the process, up-going levels wind up approaching $[m,N+1-m]$ with m' increased by 1, while down-going levels arrive at $[m+1,N-m]$ with m increased by 1. This can be summarized by combining the series (17a) and (17b) for $N\geqslant0$ into a two-component vector

$$\begin{pmatrix}\mathcal{A}_{N+1}^{(\uparrow)}(d,\varphi;\xi,\eta) \\ \mathcal{A}_{N+1}^{(\downarrow)}(d,\varphi;\xi,\eta)\end{pmatrix}=\begin{pmatrix}\eta & 0 \\ 0 & \xi\end{pmatrix}\begin{pmatrix}-d & a \\ a & d\end{pmatrix}\begin{pmatrix}\mathcal{A}_N^{(\uparrow)}(d,\varphi;\xi,\eta) \\ \mathcal{A}_N^{(\downarrow)}(d,\varphi;\xi,\eta)\end{pmatrix}. \tag{18}$$

The phase information (5) will be incorporated into η and ξ. Suppose N avoided crossings have been traversed and consider the possible fates of path j after negotiating the next avoided crossing. If this path emerges on the down-going level, the next intersection it approaches is still marked by the same value of m' but by the next highest m; one more factor of ξ is acquired in the second line of Eq. (18). The dynamical phase as defined in Eqs. (13) and (14) does not

change. If, on the other hand, the path emerges on the up-going level, the relevant value of m does not change, whereas m' increases by unity and *the path's dynamical phase increases by $m\varphi$* in the exponent in Eq. (11); this is illustrated in Fig. 2. Thus the phase associated with each path passing through $[m,m']$ acquires no extra phase upon its advance to $[m+1,m']$, but does pick up a phase factor $e^{im\varphi}$ if it advances to $[m,m'+1]$. The amplitudes for successive generations then satisfy the recursion relations

$$\mathcal{A}^{(\uparrow)}_{mm'}(d,\varphi)=[-d\mathcal{A}^{(\uparrow)}_{m,m'-1}(d,\varphi)+a\mathcal{A}^{(\downarrow)}_{m,m'-1}(d,\varphi)]e^{im\varphi},\tag{19a}$$

$$\mathcal{A}^{(\downarrow)}_{mm'}(d,\varphi)=a\mathcal{A}^{(\uparrow)}_{m-1,m'}(d,\varphi)+d\mathcal{A}^{(\downarrow)}_{m-1,m'}(d,\varphi),\tag{19b}$$

which completely determine the system's evolution.

To encode this information into Eq. (18), we regard η as an operator $\hat{\eta}$ that measures the power of ξ in each term of the polynomials $\mathcal{A}^{(\uparrow)}_N(d,\varphi;\xi,\eta)$ and $\mathcal{A}^{(\downarrow)}_N(d,\varphi;\xi,\eta)$ and effects the replacement $\xi\to e^{i\varphi}\xi$. This behavior in turn produces

$$\hat{\eta}\xi^m\to e^{im\varphi}\xi^m\hat{\eta},\tag{20}$$

which results in the correct phase factors being appended to all paths. Both expansion parameters ξ and η in Eq. (18) will henceforth be treated as operators and expressed in terms of noncommuting, positionlike and momentumlike operators $\hat{x}$ and $\hat{p}$:

$$\hat{\xi}\equiv e^{i\hat{x}},\quad \hat{\eta}\equiv e^{i\varphi\hat{p}},\quad [\hat{x},\hat{p}]=i.\tag{21}$$

For an arbitrary polynomial function $f(\hat{x})$ the translation property

$$e^{+i\varphi\hat{p}}f(\hat{x})e^{-i\varphi\hat{p}}=f(\hat{x}+\varphi)\tag{22}$$

implies

$$e^{+i\varphi\hat{p}}e^{i\hat{x}}e^{-i\varphi\hat{p}}=e^{i\hat{x}}e^{i\varphi}\quad\text{or}\quad \hat{\eta}\hat{\xi}=e^{i\varphi}\hat{\xi}\hat{\eta},\tag{23}$$

so the substitutions (21) indeed produce Eq. (20).

Matters are greatly simplified if we now generalize the procedure of Ref. [6] in order to treat all up-going amplitudes $\mathcal{A}^{(\uparrow)}_{mm'}(d,\varphi)$ over the entire grid as a single entity and likewise treat all down-going amplitudes $\mathcal{A}^{(\downarrow)}_{mm'}(d,\varphi)$ as a second distinct object. We therefore define generating functions of the operators $\hat{x}$ and $\hat{p}$ that extend the sums in Eqs. (17a) and (17b) to all values $N\geq 0$, i.e., to all $m\geq 0$ and $m'\geq 0$,

$$\mathcal{A}^{(\uparrow)}(d,\varphi;\hat{x},\hat{p})\equiv\sum_{N=0}^{\infty}\mathcal{A}^{(\uparrow)}_N(d,\varphi;\hat{\xi},\hat{\eta})=\sum_{m=0}^{\infty}\sum_{m'=0}^{\infty}$$
$$\times\mathcal{A}^{(\uparrow)}_{mm'}(d,\varphi)e^{im\hat{x}}e^{im'\varphi\hat{p}},\tag{24a}$$

$$\mathcal{A}^{(\downarrow)}(d,\varphi;\hat{x},\hat{p})\equiv\sum_{N=0}^{\infty}\mathcal{A}^{(\downarrow)}_N(d,\varphi;\hat{\xi},\hat{\eta})=\sum_{m=0}^{\infty}\sum_{m'=0}^{\infty}$$
$$\times A^{(\downarrow)}_{mm'}(d,\varphi)e^{im\hat{x}}e^{im'\varphi\hat{p}}.\tag{24b}$$

The initial condition is given in Eq. (9). Now summing Eq. (18) over N, the recursion relations (19) translate into a propagation statement that applies to the whole map yet is condensed into the form of a two-state mixing problem

$$\begin{pmatrix}\mathcal{A}^{(\uparrow)}(d,\varphi;\hat{x},\hat{p})\\\mathcal{A}^{(\downarrow)}(d,\varphi;\hat{x},\hat{p})\end{pmatrix}=\begin{pmatrix}1\\0\end{pmatrix}+\begin{pmatrix}e^{i\varphi\hat{p}}&0\\0&e^{i\hat{x}}\end{pmatrix}\begin{pmatrix}-d&a\\a&d\end{pmatrix}$$
$$\times\begin{pmatrix}\mathcal{A}^{(\uparrow)}(d,\varphi;\hat{x},\hat{p})\\\mathcal{A}^{(\downarrow)}(d,\varphi;\hat{x},\hat{p})\end{pmatrix},\tag{25}$$

with

$$d^2+a^2=1,\quad 0\leq d,a\leq 1.\tag{26}$$

The inhomogeneous "seed" term for $m=m'=0$ must appear here to make up for the absence of $N=0$ on the left-hand side in Eq. (18). Notice that the factors in Eqs. (24a) and (24b) are ordered "normally," so that all factors involving the operator $\hat{p}$ lie to the right of those with $\hat{x}$. This is significant because the two coupled equations (25) cannot be solved as a simple 2×2 eigenvalue problem: The operator $e^{i\varphi\hat{p}}$ appears to the *left* of the amplitudes, which greatly complicates an analysis by diagonalization.

C. Series solutions and generating functions for the amplitudes

The matrix containing the phase-generating factors $e^{i\varphi\hat{p}}$ and $e^{i\hat{x}}$ in Eq. (25) increments the power of either $\hat{\eta}$ or $\hat{\xi}$ in the generating functions on the right-hand side by one. This increases $N=m+m'$ by one: Every state evolves through one more avoided crossing. Recursive substitution of the two-vector into itself N times yields the evolution through N generations explicitly. This produces, in effect, a Dyson series: The initial $N=0$ term generates the amplitudes for successive $N>0$,

$$\begin{pmatrix}\mathcal{A}^{(\uparrow)}_N(d,\varphi;\hat{\xi},\hat{\eta})\\\mathcal{A}^{(\downarrow)}_N(d,\varphi;\hat{\xi},\hat{\eta})\end{pmatrix}=\left[\begin{pmatrix}\hat{\eta}&0\\0&\hat{\xi}\end{pmatrix}\begin{pmatrix}-d&a\\a&d\end{pmatrix}\right]^N\begin{pmatrix}1\\0\end{pmatrix}.\tag{27}$$

This generating function is exact and, together with Eqs. (17) and (23), provides the basis for a computational scheme for obtaining amplitudes and probabilities in this model. Numerical results are presented in Secs. III–V.

Equation (27) is similar in structure to the PWeb result, Eq. (39) of Ref. [6], in which all interference effects are ignored [13]. The present result, however, is less amenable to a statistical analysis. To extract the paths' relative dynamical phases, all products must be brought into the normal ordering of Eqs. (24). Owing to the difficulty of disentangling the various factors of $e^{i\varphi\hat{p}}$ and $e^{i\hat{x}}$ for all 2^N paths, Eq. (27) for arbitrary N cannot be analyzed in a straightforward way in all cases.

On the other hand, Eq. (25) is a simple pair of operator equations that can be solved exactly. One has only to invert the matrix

$$\hat{\mathbf{G}}^{-1}\equiv\begin{pmatrix}1+d\hat{\eta}&-a\hat{\eta}\\-a\hat{\xi}&1-d\hat{\xi}\end{pmatrix},\tag{28}$$

taking into account the noncommutativity of $\hat{\eta}$ and $\hat{\xi}$ via Eqs. (21) and (23), to find

$$\begin{pmatrix} \mathcal{A}^{(\uparrow)}(d,\varphi;\hat{\xi},\hat{\eta}) \\ \mathcal{A}^{(\downarrow)}(d,\varphi;\hat{\xi},\hat{\eta}) \end{pmatrix} = \hat{\mathbf{G}} \begin{pmatrix} 1 \\ 0 \end{pmatrix}$$

$$= \begin{pmatrix} [1+d(\hat{\eta}-\hat{\xi}e^{i\varphi})-\hat{\eta}\hat{\xi}]^{-1}(1-d\hat{\xi}e^{i\varphi}) \\ [1+d(\hat{\eta}e^{-i\varphi}-\hat{\xi})-\hat{\xi}\hat{\eta}]^{-1}a\hat{\xi} \end{pmatrix}.$$

$$(29)$$

The operator matrix $\hat{\mathbf{G}}$ plays the role of a propagator. The generating functions (29) are also exact: When combined with the definitions (24a) and (24b), they yield all amplitudes over the entire grid. The analog of this result for the PWeb model, where noncommutativity of $\hat{\xi}$ and $\hat{\eta}$ is not an issue, is given in the Appendix.

A symmetry property of the down-going amplitudes is revealed by examining the kernel of their generator in Eq. (29). After passing the factor $\hat{\xi}$ to the left of $[\ ]^{-1}$ in $\mathcal{A}^{(\downarrow)}(d,\varphi;\hat{\xi},\hat{\eta})$, one has

$$\mathcal{A}^{(\downarrow)}(d,\varphi;\hat{\xi},\hat{\eta}) = a\hat{\xi}g(d,\varphi;\hat{\xi},\hat{\eta})$$

$$= \sum_{m=0}^{\infty}\sum_{m'=0}^{\infty}\mathcal{A}^{(\downarrow)}_{mm'}(d,\varphi)\hat{\xi}^m\hat{\eta}^{m'}, \quad (30)$$

where

$$g(d,\varphi;\hat{\xi},\hat{\eta}) = [1+d(\hat{\eta}-\hat{\xi})-\hat{\eta}\hat{\xi}]^{-1}$$

$$= a^{-1}\sum_{r=0}^{\infty}\sum_{s=0}^{\infty}\mathcal{A}^{(\downarrow)}_{r+1,s}(d,\varphi)\hat{\xi}^r\hat{\eta}^s \quad (31)$$

and the indices have been renamed $r=m-1$ and $s=m'$. The kernel (31) appears to be symmetric under interchange of $\hat{\xi}$ and $\hat{\eta}$ if d also flips sign. This turns out to be the case even though $\hat{\eta}\hat{\xi}\neq\hat{\xi}\hat{\eta}$. Interchanging $\hat{\xi}$ and $\hat{\eta}$, and then r and s, in Eq. (31) yields

$$g(d,\varphi;\hat{\eta},\hat{\xi}) = [1-d(\hat{\eta}-\hat{\xi})-\hat{\xi}\hat{\eta}]^{-1}$$

$$= a^{-1}\sum_{r=0}^{\infty}\sum_{s=0}^{\infty}\mathcal{A}^{(\downarrow)}_{s+1,r}(d,\varphi)\hat{\eta}^s\hat{\xi}^r. \quad (32)$$

On the other hand, the series expansion of $g(d,\varphi;\hat{\xi},\hat{\eta})$ is homogenous in powers of $(\hat{\eta}-\hat{\xi})$ and $(\hat{\eta}\hat{\xi})$. Hence an exchange of $\hat{\eta}$ and $\hat{\xi}$ *and* a sign change of d should produce the same joint weighting of powers $\hat{\xi}^r\hat{\eta}^s$ as in Eq. (31), if all factors $\hat{\xi}$ are instead moved to the *right* and all factors of $\hat{\eta}$ are moved to the *left*:

$$g(-d,\varphi;\hat{\eta},\hat{\xi}) = [1+d(\hat{\eta}-\hat{\xi})-\hat{\xi}\hat{\eta}]^{-1}$$

$$= a^{-1}\sum_{r=0}^{\infty}\sum_{s=0}^{\infty}\mathcal{A}^{(\downarrow)}_{r+1,s}(d,\varphi)\hat{\eta}^s\hat{\xi}^r. \quad (33)$$

Comparing the amplitudes in Eqs. (32) and (33) we obtain the relation

$$\mathcal{A}^{(\downarrow)}_{m'+1,m-1}(d,\varphi) = \mathcal{A}^{(\downarrow)}_{m,m'}(-d,\varphi)$$

$$= (-1)^{m+m'-1}\mathcal{A}^{(\downarrow)}_{m,m'}(d,\varphi), \quad (34)$$

which holds independently of d and φ. The sign $(-1)^{N-1}$ follows from the fact that a down-going level can only be reached from the up-going initial state through an odd number of adiabatic transitions, so that the number of powers of d must be odd (even) if $N=m+m'$ is even (odd). Equation (34) expresses a symmetry (to within a phase) of the down-going amplitudes about the origin of a grid shifted to intersection $[1,0']$. Such a relation is identical to that found for down-going-level probabilities in the PWeb model [14].

In a similar way, the upgoing amplitudes of Eq. (29) can be rewritten as

$$\mathcal{A}^{(\uparrow)}(d,\varphi;\hat{\xi},\hat{\eta}) = \hat{\eta}[1+d(\hat{\eta}-\hat{\xi})-\hat{\xi}\hat{\eta}]^{-1}(1-d\hat{\xi})\hat{\eta}^{-1}$$

$$= 1+\hat{\eta}[1+d(\hat{\eta}-\hat{\xi})-\hat{\xi}\hat{\eta}]^{-1}(\hat{\xi}-d), \quad (35)$$

where this time a factor of $\hat{\eta}$ has been swept to the left of the entire expression. Although the coefficients $\mathcal{A}^{(\uparrow)}_{mm'}(d,\varphi)$ depend on a kernel $[1+d(\hat{\eta}-\hat{\xi})-\hat{\xi}\hat{\eta}]^{-1}$ similar to $g(d,\varphi;\hat{\xi},\hat{\eta})$, a simple symmetry like Eq. (34) is not forthcoming owing to the factor $(\hat{\xi}-d)$ in Eq. (35).

Specific cases and limits emerge directly from Eqs. (30), (31), and (35). At intersections with the $m=0$ level, the amplitudes are the coefficients of $\hat{\xi}^0$ (equivalently one can set $\hat{\xi}=0$),

$$\mathcal{A}^{(\uparrow)}_{(m=0)}(d,\varphi;\hat{\xi},\hat{\eta}) = [1+d\hat{\eta}]^{-1} \Rightarrow \mathcal{A}^{(\uparrow)}_{0m'}(d,\varphi) = (-d)^{m'}$$

$$(36a)$$

and

$$\mathcal{A}^{(\downarrow)}_{(m=0)}(d,\varphi;\hat{\xi},\hat{\eta}) = 0 \Rightarrow \mathcal{A}^{(\downarrow)}_{0m'}(d,\varphi) = 0. \quad (36b)$$

The sequence of intersections $[m=0, m'\geq 0]$ represents successive diabatic transitions, defining a "purely diabatic path," from which population leaks exponentially as $\mathcal{P}^{(\uparrow)}_{0m'}(d,\varphi) = D^{m'}$, as in the PWeb [6] and Demkov-Osherov [5] models. Since no levels are ever populated above this sequence on the grid, down-going levels have zero amplitude until they cross the $m=0$ level. Similarly, no up-going levels are populated below their intersection with $m'=0$ *except* the initial $m=0$ level itself. The $m'=0$ amplitudes are the coefficients of $\hat{\eta}^0$ (or one can set $\hat{\eta}=0$),

$$\mathcal{A}^{(\uparrow)}_{(m'=0)}(d,\varphi;\hat{\xi},\hat{\eta}) = 1 \Rightarrow \mathcal{A}^{(\uparrow)}_{m0}(d,\varphi;\hat{\xi},\hat{\eta}) = \delta_{m0}$$

$$(37a)$$

and

$$\mathcal{A}^{(\downarrow)}_{(m'=0)}(d,\varphi;\hat{\xi},\hat{\eta}) = a\hat{\xi}[1-d\hat{\xi}]^{-1} \Rightarrow \mathcal{A}^{(\downarrow)}_{m0}(d,\varphi;\hat{\xi},\hat{\eta})$$

$$= \begin{cases} 0, & m=0 \\ ad^{m-1}, & m>0. \end{cases} \quad (37b)$$

Other specific cases, for higher values of m and m', can be obtained explicitly for intersections between these extremes, but their forms get progressively more complicated.

In the diabatic limit $d \to 1$ (or $a \to 0$), the generating functions give

$$\mathcal{A}^{(\uparrow)}(d,\varphi;\hat{\xi},\hat{\eta}) \xrightarrow[d \to 1]{} [1+\hat{\eta}]^{-1}$$

$$\Rightarrow \mathcal{A}^{(\uparrow)}_{mm'}(1,\varphi) = \delta_{m0}(-1)^{m'}, \quad (38a)$$

$$\mathcal{A}^{(\downarrow)}(d,\varphi;\hat{\xi},\hat{\eta}) \xrightarrow[d \to 1]{} 0 \Rightarrow \mathcal{A}^{(\downarrow)}_{mm'}(1,\varphi)=0, \quad (38b)$$

since the only path taken at very large ramp rates or for very small coupling is the purely diabatic one, Eq. (36). In the opposite, adiabatic limit $d \to 0$ ($a \to 1$), one finds instead

$$\mathcal{A}^{(\uparrow)}(d,\varphi;\hat{\xi},\hat{\eta}) \xrightarrow[d \to 0]{} [1-\hat{\eta}\hat{\xi}]^{-1}$$

$$\Rightarrow \mathcal{A}^{(\uparrow)}_{mm'}(0,\varphi) = \delta_{m,m'}e^{im'(m'+1)\varphi/2}, \quad (39a)$$

$$\mathcal{A}^{(\downarrow)}(d,\varphi;\hat{\xi},\hat{\eta}) \xrightarrow[d \to 0]{} \hat{\xi}[1-\hat{\eta}\hat{\xi}]^{-1}$$

$$\Rightarrow \mathcal{A}^{(\downarrow)}_{mm'}(0,\varphi) = \delta_{m,m'+1}e^{im'(m'+1)\varphi/2}. \quad (39b)$$

Equations (39) single out the ''purely adiabatic'' path running through the center of the grid; it alternates between up- and down-going levels, which approach intersections $[m,m]$ (N even) and $[m,m-1]$ (N odd), respectively.

D. Integral representations of the amplitudes

In order to obtain the amplitudes in closed form, we solve the pair of equations (25) by matching like powers $\hat{\eta}^{m'} = e^{im'\varphi\hat{p}}$. The coefficient of each power of $e^{im'\varphi\hat{p}}$ in the generating functions (24) is itself a partial generating function, a series in powers of $e^{i\hat{x}}$:

$$\mathcal{A}^{(\uparrow)}(d,\varphi;\hat{x},\hat{p}) = \sum_{m'=0}^{\infty} F_{m'}(d,\varphi;\hat{x})e^{im'\varphi\hat{p}}, \quad (40a)$$

$$\mathcal{A}^{(\downarrow)}(d,\varphi;\hat{x},\hat{p}) = \sum_{m'=0}^{\infty} G_{m'}(d,\varphi;\hat{x})e^{im'\varphi\hat{p}}, \quad (40b)$$

where

$$F_{m'}(d,\varphi;\hat{x}) \equiv \sum_{m=0}^{\infty} \mathcal{A}^{(\uparrow)}_{mm'}(d,\varphi)e^{im\hat{x}}, \quad (41a)$$

$$G_{m'}(d,\varphi;\hat{x}) \equiv \sum_{m=0}^{\infty} \mathcal{A}^{(\downarrow)}_{mm'}(d,\varphi)e^{im\hat{x}}. \quad (41b)$$

Each term on the right-hand side of the first line of Eq. (25) acquires an additional power of $e^{i\varphi\hat{p}}$, whereas the second line does not. The terms on both sides of Eqs. (40a) and (40b) are therefore related by

$$F_{m'+1}(d,\varphi;\hat{x})e^{i(m'+1)\varphi\hat{p}} = e^{i\varphi\hat{p}}[-dF_{m'}(d,\varphi;\hat{x})$$
$$+aG_{m'}(d,\varphi;\hat{x})]e^{im'\varphi\hat{p}},$$
$$(42a)$$

$$G_{m'}(d,\varphi;\hat{x})e^{im'\varphi\hat{p}} = e^{i\hat{x}}[aF_{m'}(d,\varphi;\hat{x})$$
$$+dG_{m'}(d,\varphi;\hat{x})]e^{im'\varphi\hat{p}}. \quad (42b)$$

The solution of these equations using Eq. (22) yields a recursion relation among the up-going partial generating functions:

$$F_{m'+1}(d,\varphi;\hat{x}) = \left(\frac{e^{i(\hat{x}+\varphi)}-d}{1-de^{i(\hat{x}+\varphi)}} \right) F_{m'}(d,\varphi;\hat{x}+\varphi), \quad (43a)$$

$$G_{m'}(d,\varphi;\hat{x}) = \left(\frac{a}{e^{-i\hat{x}}-d} \right) F_{m'}(d,\varphi;\hat{x}). \quad (43b)$$

Finally, the amplitudes of up-going levels crossing the $m'=0$ level are known [from, e.g., the coefficient of $\hat{\eta}^0$ in Eq. (35)] to be nonzero only for $m=0$, so $F_{0'}(d,\varphi;\hat{x})=1$. Then iterating Eq. (43a) yields

$$F_{m'}(d,\varphi;\hat{x}) = \prod_{k=1}^{m'} \frac{e^{ik\varphi}e^{i\hat{x}}-d}{1-de^{ik\varphi}e^{i\hat{x}}} \quad (44a)$$

and

$$G_{m'}(d,\varphi;\hat{x}) = \frac{ae^{i\hat{x}}}{1-de^{i\hat{x}}} \prod_{k=1}^{m'} \frac{e^{ik\varphi}e^{i\hat{x}}-d}{1-de^{ik\varphi}e^{i\hat{x}}} \quad (44b)$$

for all $m' \geq 0$, if we adopt the convention that the null-range product $\prod_1^0$ equals unity.

From the definitions (41), the amplitudes $\mathcal{A}^{(\uparrow)}_{mm'}(d,\varphi)$ and $\mathcal{A}^{(\downarrow)}_{mm'}(d,\varphi)$ now follow from extracting the various integral powers of $e^{i\hat{x}}$ from $F_{m'}(d,\varphi;\hat{x})$ and $G_{m'}(d,\varphi;\hat{x})$. For this purpose it suffices to treat $\hat{x}$ as just a variable θ and to Fourier analyze Eq. (44a):

$$\mathcal{A}^{(\uparrow)}_{mm'}(d,\varphi) = \frac{1}{2\pi} \int_0^{2\pi} d\theta \, e^{-im\theta} \prod_{k=1}^{m'} \frac{e^{ik\varphi}e^{i\theta}-d}{1-de^{ik\varphi}e^{i\theta}}. \quad (45)$$

Note that this and all subsequent representations are invariant under $\theta \to \theta+2\pi$. This integral will first be evaluated explicitly by analyzing its poles, then approximated as an integral representation of well-known functions. Once the up-going amplitudes $\mathcal{A}^{(\uparrow)}_{mm'}(d,\varphi)$ are known, the down-going ones follow from, e.g.,

$$\mathcal{A}^{(\downarrow)}_{mm'}(d,\varphi) = a^{-1}[\mathcal{A}^{(\uparrow)}_{m,m'+1}(d,\varphi)e^{-im\varphi}+d\mathcal{A}^{(\uparrow)}_{mm'}(d,\varphi)] \quad (46)$$

or equivalent recursion relations obtained from Eqs. (19a) and (19b).

The substitution $z \equiv e^{i\theta}$ converts Eq. (45) to an integral over a counterclockwise contour of unit modulus in the complex-z plane:

$$\mathcal{A}_{mm'}^{(\uparrow)}(d,\varphi) = \frac{1}{2\pi i} \oint_{|z|=1} dz \frac{1}{z^{m+1}} \prod_{k=1}^{m'} \frac{e^{ik\varphi}z - d}{1 - de^{ik\varphi}z}. \tag{47}$$

The simple poles at $z = e^{-ik\varphi}/d$ have $|z| > 1$ when $d < 1$, so only the pole of order $m+1$ at $z = 0$ contributes to Eq. (47):

$$\mathcal{A}_{mm'}^{(\uparrow)}(d,\varphi) = \frac{1}{m!} \frac{d^m}{dz^m} \left[\prod_{k=1}^{m'} \frac{e^{ik\varphi}z - d}{1 - de^{ik\varphi}z} \right]_{z=0}. \tag{48}$$

This result also follows by simple inspection of Eqs. (44a) and (41a). Alternatively, using $\zeta \equiv e^{-i\theta}$ leads to

$$\mathcal{A}_{mm'}^{(\uparrow)}(d,\varphi) = \frac{1}{2\pi i} \oint_{|\zeta|=1} d\zeta \, \zeta^{m-1} \prod_{k=1}^{m'} \frac{e^{ik\varphi} - d\zeta}{\zeta - de^{ik\varphi}}, \tag{49}$$

which now has no pole at $\zeta = 0$ (if $m > 0$) and whose simple poles at $\zeta = de^{ik\varphi}$ lie within $|\zeta| < 1$ (if $d < 1$). If $m' = 0$, Eq. (49) reduces to δ_{m0}, as in Eq. (37a); otherwise

$$\mathcal{A}_{mm'}^{(\uparrow)}(d,\varphi) = a^2 d^{m-m'} \sum_{\tilde{k}=1}^{m'} e^{im\tilde{k}\varphi} \prod_{k=1}^{m'} \delta_{k\tilde{k}}' \frac{1 - de^{i(\tilde{k}-k)\varphi}}{e^{i(\tilde{k}-k)\varphi} - 1}, \tag{50}$$

where $\delta_{k\tilde{k}}'$ is the complementary Kronecker delta (it vanishes only if $k = \tilde{k}$; otherwise it equals unity).

Though exact, the general equations (48) and (50) are inconvenient for purposes of analysis. But note that each factor in the product in Eq. (45) has unit modulus and an argument of the form $2\Theta(d;\vartheta) + \vartheta$, where

$$\Theta(d;\vartheta) = \tan^{-1}\left(\frac{\sin\vartheta}{\cos\vartheta - d} \right) - \vartheta, \tag{51}$$

with $\vartheta = \theta + k\varphi$. The entire integrand is therefore a *single* phase factor with a sum of θ-dependent phases. With $\theta' \equiv \theta + \varphi$, the amplitudes (45) become

$$\mathcal{A}_{mm'}^{(\uparrow)}(d,\varphi) = \Phi_1 \frac{1}{2\pi} \int_0^{2\pi} d\theta' \exp\left[i\left\{ 2\sum_{k=0}^{m'-1} \Theta(d;\theta'+k\varphi) \right. \right.$$

$$\left. \left. + (m'-m)\theta' \right\} \right], \tag{52}$$

where the phase prefactor is

$$\Phi_1 = e^{i[m + m'(m'-1)/2]\varphi}. \tag{53}$$

Figure 3 shows the phase function $\Theta(d;\vartheta)$ over the whole range of d: It has a single oscillation with extremal values $\pm[\frac{1}{2}\pi - \cos^{-1}(d)]$ at $\vartheta = \pm\cos^{-1}(d)$, but becomes more nearly triangular in the diabatic limit. Its limiting forms are
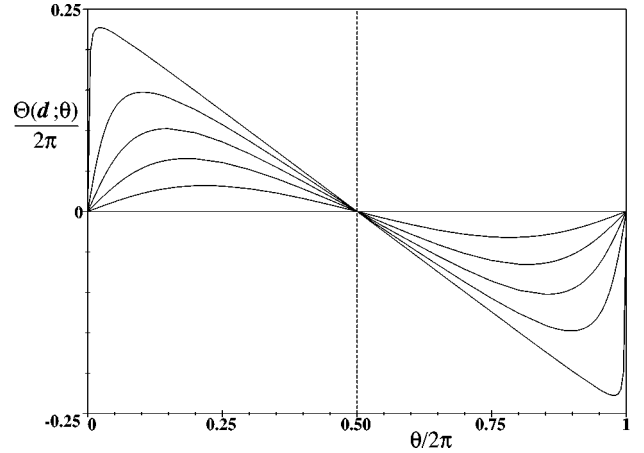
FIG. 3. A log-log plot of the phase function $\Theta(d;\theta)$ [Eq. (51)] vs $\theta(\mathrm{mod}\,2\pi)$ for $d = 0$, 0.2, 0.4, 0.6, 0.8, and 0.99. $\Theta(d;\theta)$ changes from a sinusoidal form at $d \approx 0$ to a sawtooth as $d \to 1$.

$$\Theta(d;\vartheta) \xrightarrow[d\to 0]{} d\sin\vartheta + O(d^2) \tag{54}$$

and

$$\Theta(d;\vartheta) \xrightarrow[d\to 1]{} \tfrac{1}{2}\pi - \tfrac{1}{2}\vartheta - \delta\cot(\tfrac{1}{2}\vartheta) + O(\delta^2), \tag{55'}$$

$$\delta \equiv \frac{1-d}{1+d}, \tag{55}$$

where Eq. (55) is an asymptotic expansion good for $\sin^2(\frac{1}{2}\vartheta) \gg \frac{1}{2}\delta$. More generally, Eq. (51) can be expanded as a convergent Taylor series in d:

$$\Theta(d;\vartheta) = \sum_{n=1}^{\infty} \frac{1}{n} d^n \sin(n\vartheta). \tag{56}$$

Then the coefficients of d^n in the integrand's exponent comprise a sum of m' shifted phases,

$$\sum_{k=0}^{m'-1} \sin(n\theta' + kn\varphi) = c_n(m',\varphi)\sin(n\theta''), \tag{57}$$

where

$$c_n(m',\varphi) = \frac{\sin(\frac{1}{2}m'n\varphi)}{\sin(\frac{1}{2}n\varphi)} \tag{58}$$

and $\theta'' \equiv \theta' + \frac{1}{2}(m'-1)\varphi$. Insertion of Eqs. (56)–(58) into the amplitudes (52) yields

$$\mathcal{A}_{mm'}^{(\uparrow)}(d,\varphi) = \Phi_2 \frac{1}{2\pi} \int_0^{2\pi} d\theta''$$

$$\times \exp\left[i\left\{ \sum_{n=1}^{\infty} \frac{2}{n} d^n c_n(m',\varphi)\sin(n\theta'') \right. \right.$$

$$\left. \left. + (m'-m)\theta'' \right\} \right], \tag{59}$$

with

$$\Phi_2 = \Phi_1 e^{i[(m-m')(m'-1)/2]\varphi} = e^{i[m(m'+1)/2]\varphi}, \qquad (60)$$

which is still an exact result. Note that when $d=0$, Eq. (60) reproduces the correct phase for the limit (39a). Equation (59), which suggests an integral representation of a kind of ''hyper-Bessel'' function, simplifies to known representations in the limits (54) and (55).

III. CONSTRUCTIVE INTERFERENCE

In the particular case of totally constructive interference, in the sense that $\varphi \to 0 (\mathrm{mod}\, 2\pi)$, Eq. (49) can be evaluated directly for any value of d. For $m>0$ the integral has one pole of order m' at $\zeta = d$, which yields

$$\mathcal{A}_{mm'}^{(\uparrow)}(d,0) = \sum_{k=1}^{m} \binom{m-1}{k-1}\binom{m'}{k}(-1)^{m'-k}a^{2k}d^{m+m'-2k}. \qquad (61a)$$

This is precisely the form that one would obtain for $\mathcal{P}_{mm'}^{(\uparrow)}(d,0)$ by following the derivation in Ref. [6], if one were to replace the sum of different paths' probabilities considered there with a sum over the path amplitudes of Sec. II A here [15,16]. Similar reasoning then leads to

$$\mathcal{A}_{mm'}^{(\downarrow)}(d,0) = \sum_{k=1}^{m} \binom{m-1}{k-1}\binom{m'}{k-1}$$
$$\times (-1)^{m'-k-1}a^{2k-1}d^{m+m'-2k+1}. \qquad (61b)$$

The probabilities for $\varphi=0$ and $m>0$ are now expressible as hypergeometric functions [15]

$$\mathcal{P}_{mm'}^{(\uparrow)}(d,0) = D^{m+m'} |_2F_1(-m,-m';1;-A/D)$$
$$- {}_2F_1(1-m,-m';1;-A/D)|^2, \qquad (62a)$$

$$\mathcal{P}_{mm'}^{(\downarrow)}(d,0) = AD^{m+m'-1} |_2F_1(1-m,-m';1;-A/D)|^2, \qquad (62b)$$

with $D=d^2$ and $A=1-d^2$. For $m=0$, Eqs. (48) and (46) give $\mathcal{A}_{0m'}^{(\uparrow)}(d,\varphi)=(-d)^{m'}$ and $\mathcal{A}_{0m'}^{(\downarrow)}(d,\varphi)=0$, as in Eqs. (36a) and (36b).

In Fig. 4 we present contour plots of $\mathcal{P}_{mm'}^{(\uparrow)}(d,0)$ and $\mathcal{P}_{mm'}^{(\downarrow)}(d,0)$ covering most of the range of values of d. The adiabatic $(d=0)$ limit has the single path approximated in Fig. 4(a), where $d=0.05$; the diabatic limit $(d=1$, not shown) would have only the path following $m=0$. For intermediate values of d, interference of many paths is such that non-negligible values of $\mathcal{P}_{mm'}^{(\uparrow)}(d,0)$ are confined mainly to a narrow band in the (m,m') plane, along which it decreases as $\sim 1/\sqrt{N}$. In the adiabatic limit [e.g., Figs. 4(b) and 4(c)] this band is mirrored by a weaker one, producing a nearly symmetric pattern about the purely adiabatic path. The $\mathcal{P}_{mm'}^{(\downarrow)}(d,0)$ plots, which are always symmetric about the line $m-m'=1$, have two weaker bands in all cases.

For each d, the band within which up-going states are most likely found is well approximated by the locus of intersections $[m,m']$ for which

$$\frac{m'}{m} = \frac{1+d}{1-d}. \qquad (63)$$

On a map of energy vs time, this slope is simply $dE/dt = pd$ [for a symmetric grid, Eqs. (2)]. As d increases the band ''angle,'' of which Eq. (63) is the tangent, rotates smoothly towards the purely diabatic path, from $dE/dt=0$ in the adiabatic limit to $dE/dt=p$ in the diabatic limit. Such a rotation from adiabatic- to diabatic-path directions proves to be a general feature of the AWeb probability distributions even for $\varphi \neq 0 (\mathrm{mod}\, 2\pi)$.

IV. ADIABATIC EVOLUTION

Adiabatic passage through the grid is characterized by small $D=d^2$. To lowest order in d, Eq. (54) or the $n=1$ term of Eq. (59) gives

$$\mathcal{A}_{mm'}^{(\uparrow)}(d,\varphi) = \Phi_2 \frac{1}{2\pi} \int_0^{2\pi} d\theta''$$
$$\times \exp\left[i\left\{ 2d\left(\frac{\sin(\frac{1}{2}m'\varphi)}{\sin(\frac{1}{2}\varphi)}\right)\sin\theta'' \right.\right.$$
$$\left.\left. + \cdots + (m'-m)\theta'' \right\} \right], \qquad (64)$$

the ellipsis indicating terms $\sim O(d^2)$. Equation (64) is just the integral representation of the regular Bessel function of integral order $m-m'$. Therefore, when adiabatic transitions dominate, evolution through the grid can be approximated by the probabilities

$$\mathcal{P}_{mm'}^{(\uparrow)}(d,\varphi) = \left| J_\nu\left(2d\frac{\sin(\frac{1}{2}m'\varphi)}{\sin(\frac{1}{2}\varphi)}\right) \right|^2, \quad \nu=m-m'. \qquad (65)$$

The Bessel-function behavior applies to sequences of intersections of constant $m-m'$, i.e., to loci parallel to the time axis (for a symmetric grid) and straddling the purely adiabatic path. However, because the grid is bounded by $m=0$ and $m'=0$, the argument of J_ν representing the grid boundary for $m'>m$ is $2dc_1(|\nu|;\varphi)$ (at $m=0$), while for $m'<m$ and the same $|\nu|$ it is zero (at $m'=0$). Therefore, these probability distributions are not quite symmetric about $m'=m$ even though $|J_\nu(x)|=|J_{-\nu}(x)|$; as d increases the distributions appear more ''sheared'' (in a counterclockwise sense) about $m'=m$.

In Fig. 5 we present three-dimensional and contour plots of $\mathcal{P}_{mm'}^{(\uparrow)}(d,\varphi)$ and $\mathcal{P}_{mm'}^{(\downarrow)}(d,\varphi)$ for various small values of d and a fixed value $\varphi=\frac{1}{4}\pi$, while in Fig. 6 we plot just $\mathcal{P}_{mm'}^{(\uparrow)}(d,\varphi)$ for various $\varphi(\mathrm{mod}\, 2\pi)$ and fixed $D=0.25$. [Here and in all subsequent plots of $\mathcal{P}_{mm'}^{(\uparrow)}$, and $\mathcal{P}_{mm'}^{(\downarrow)}$ we display numerical results only, not approximations, using recursion relations obtained from Eqs. (19) or, equiva-
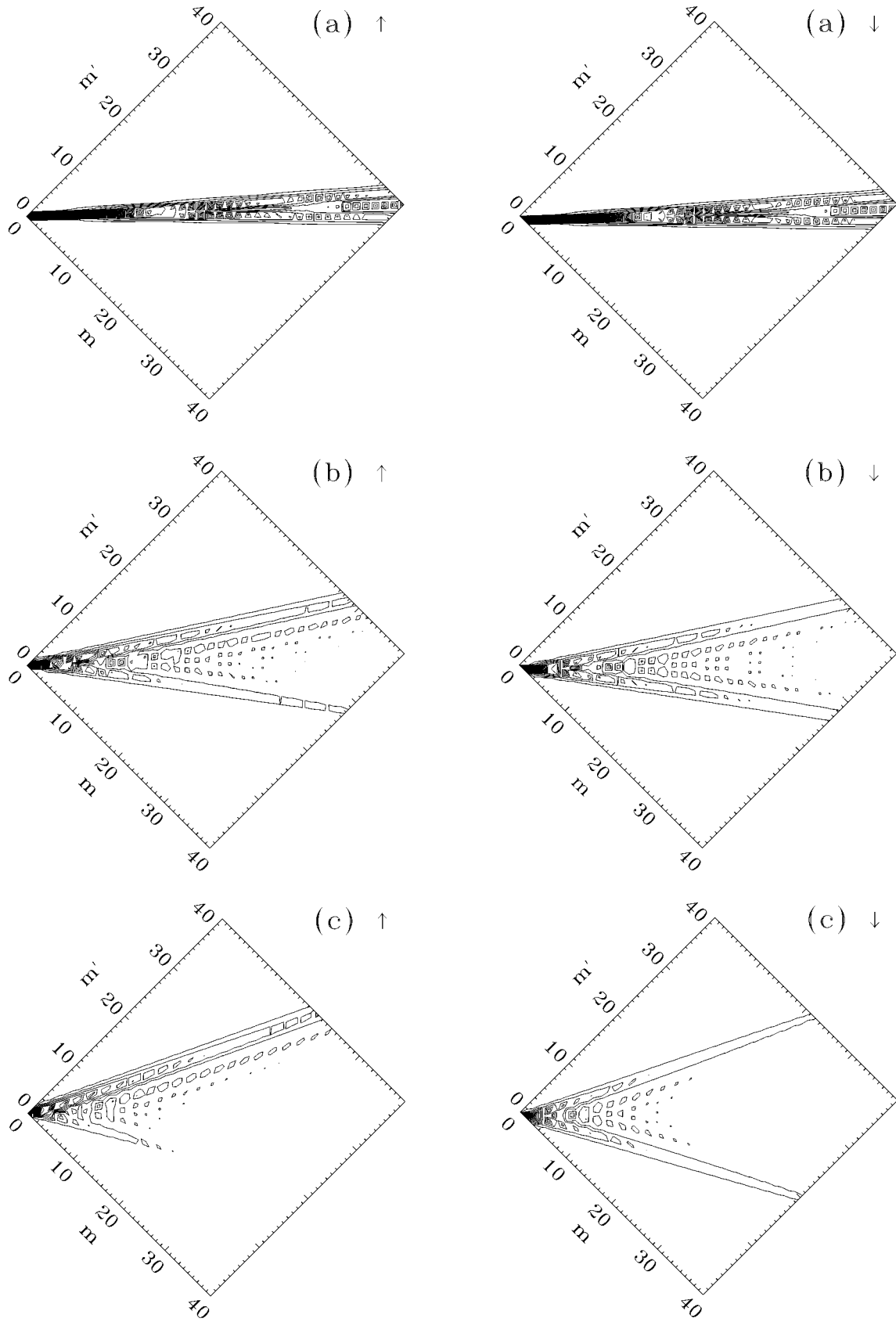
FIG. 4. Contour plots of probabilities $\mathcal{P}_{mm'}^{(\uparrow)}(d,0)$ (left) and $\mathcal{P}_{mm'}^{(\downarrow)}(d,0)$ (right) for totally constructive interference $\varphi = 0 (\mathrm{mod}\, 2\pi)$ and various values of the diabatic transition probability $D = d^2$ [Eqs. (3) and (10)]:   (a) $d = 0.05$, (b) 0.20, (c) 0.35, (d) 0.50, (e) 0.70, and (f) 0.90. Each case is plotted as probability vs (m, m') on a symmetric, discrete grid of intersections $[m, m']$, up to $N = m + m' = 80$. Contours are interpolated in steps of 0.05. The initial up-going state, $m = 0$ at the intersection with $m' = 0$, has the maximum value of unity. The horizontal axis is proportional to time, the vertical axis to energy [Eqs. (2)].

(d) ↑

(d) ↓

(e) ↑

(e) ↓

(f) ↑

(f) ↓
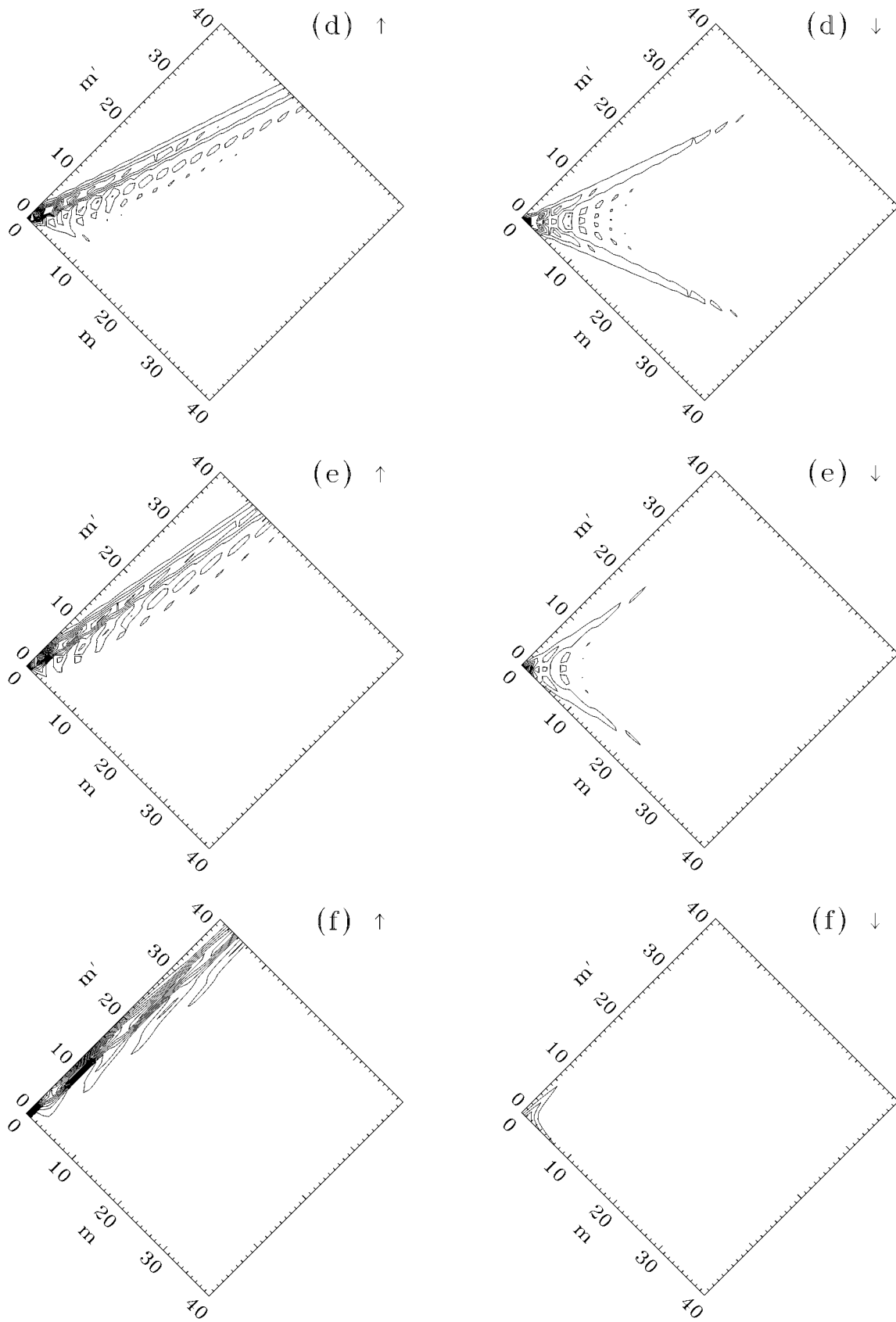
FIG. 4. (*Continued*).
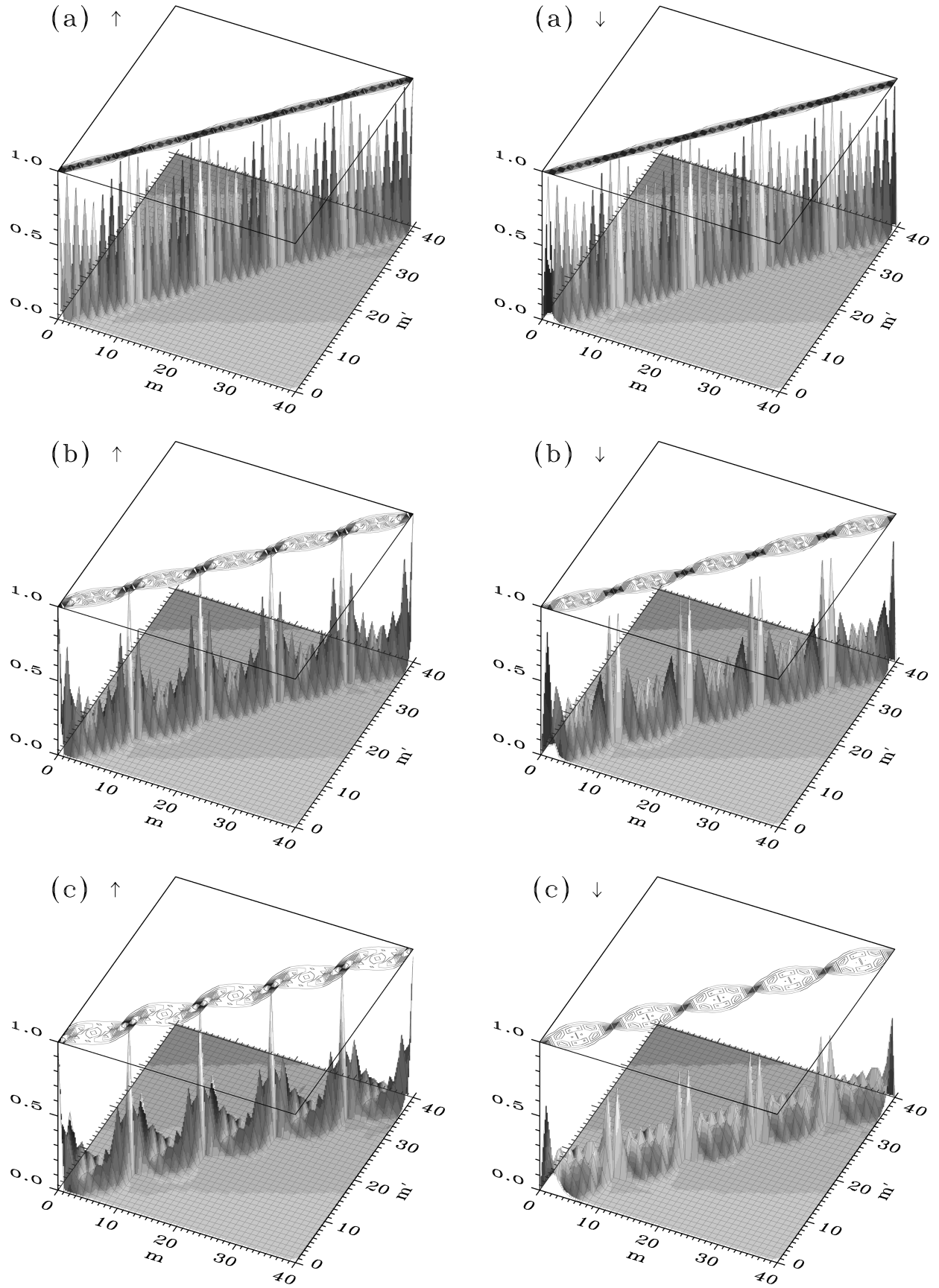
FIG. 5. Three-dimensional and contour plots of probabilities $\mathcal{P}_{mm'}^{(\uparrow)}(d,\varphi)$ (left) and $\mathcal{P}_{mm'}^{(\downarrow)}(d,\varphi)$ (right) vs (m,m') in the adiabatic approximation [cf. Eq. (65)], for fixed $\varphi = \frac{1}{4}\pi$ ($\mu = 8$) and various values of $D = d^2 < \frac{1}{2}$: (a) $d = 0.15$, (b) 0.40, and (c) 0.65. Contours are as in Fig. 4.
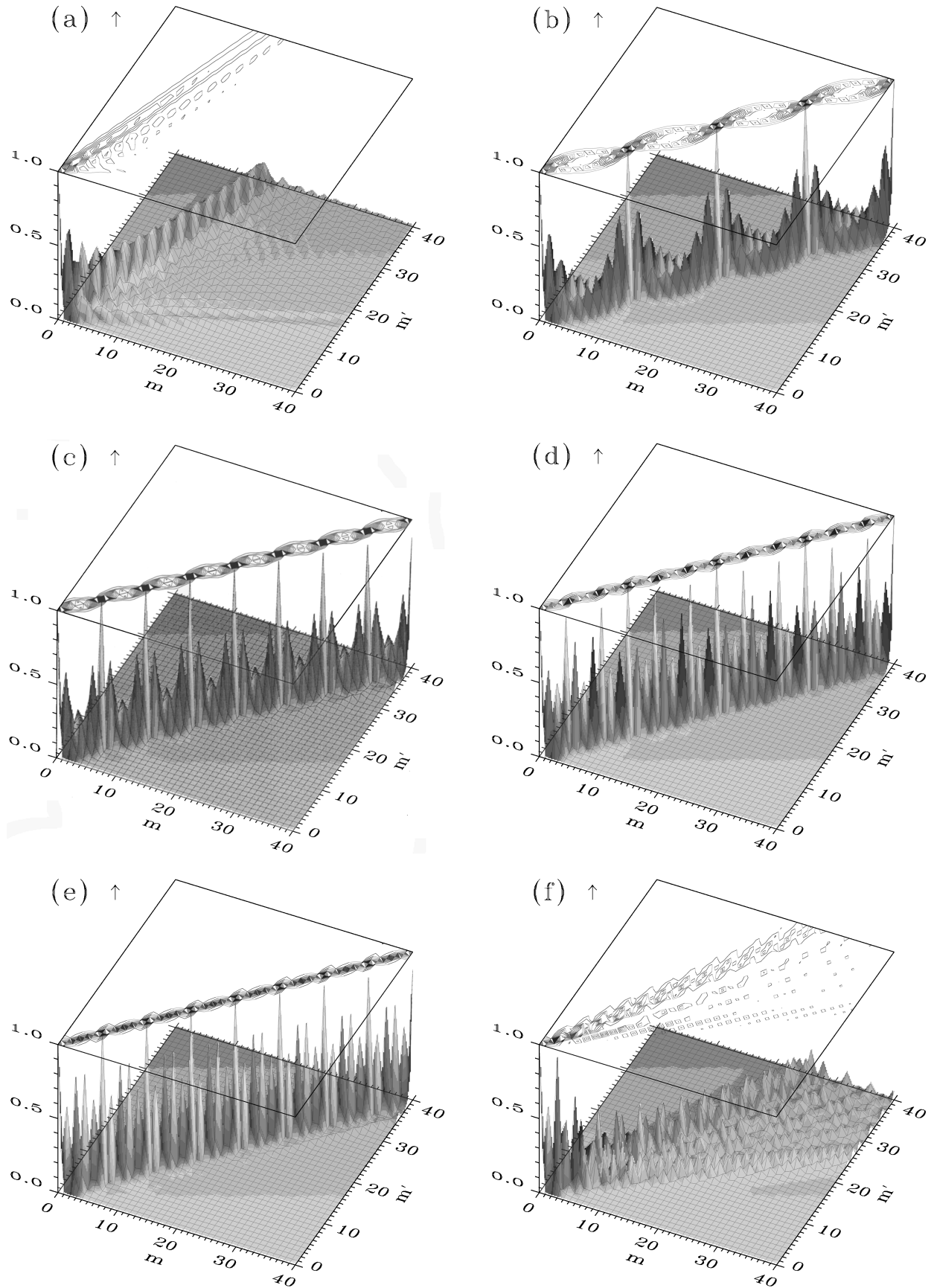
FIG. 6. Three-dimensional and contour plots of probabilities $\mathcal{P}_{mm'}^{(\uparrow)}(d,\varphi)$ vs (m,m') in the adiabatic approximation [cf. Eq. (65)] for fixed $D=0.25$ and various $\varphi(\mathrm{mod}\,2\pi)$: (a) $\varphi=0$ $(\mu\to\infty)$, (b) $\varphi=0.20\pi$ $(\mu=10)$, (c) $\varphi=0.40\pi$ $(\mu=5)$, (d) $\varphi=0.60\pi$ $(\mu=\frac{10}{3})$, (e) $\varphi=0.80\pi$ $(\mu=\frac{5}{2})$, and (f) $\varphi=\pi$ $(\mu=2)$. Contours are as in Fig. 4.

lently, Eqs. (24)–(27).] Note that the evolution typically follows a braiding pattern about the center of the grid, unless $\varphi \rightarrow 0 (\mathrm{mod} 2\pi)$ as in Fig. 4.

Figures 5 and 6 illustrate that in the adiabatic limit there is a nearly perfect *recurrence of the entire distribution* with integral period $\Delta m'$. From Eq. (65), the condition for such a revival is $\Delta m' \varphi = 0 (\mathrm{mod} 2\pi)$ if we note $J_\nu(-x) = (-1)^\nu J_\nu(x)$. This period should equal the number of action units it takes to complete one phase cycle,

$$\mu \equiv \frac{2\pi}{|\varphi(\mathrm{mod} 2\pi)|} \geq 2, \quad -\pi < \varphi(\mathrm{mod} 2\pi) < \pi, \quad (66)$$

if μ is precisely an integer. (This μ is not related to the quantum defects μ_l.) Since the period (66) applies for any order ν, we have $\Delta m = \mu$ as well, so

$$\mathcal{P}^{(\uparrow)}_{m+\mu, m'+\mu}(d, \varphi) = \mathcal{P}^{(\uparrow)}_{mm'}(d, \varphi) \quad \text{as } d \rightarrow 0. \quad (67)$$

The pattern recurs after every $\Delta N = 2\mu$ generations of anticrossings have been traversed. [The repetition occurs *in time* with $\Delta t = \mu(\varepsilon + \varepsilon')/(p - p')$, from Eq. (2a).] In particular,

$$\mathcal{P}^{(\uparrow)}_{M\mu, M\mu}(d, \varphi) = \mathcal{P}^{(\uparrow)}_{00'}(d, \varphi) = 1, \quad M = 0, 1, 2, \ldots, \quad \text{as } d \rightarrow 0; \quad (68)$$

the initial population interferes totally constructively at the "knots" of the braid. At the same points $\mathcal{P}_{mm'}(d, \varphi)$ vanishes. This is evident in all cases shown in Figs. 5 and 6(b)–6(e). Revivals in the short-time propagator of a similar model were noted in Ref. [7].

However, the m and m' period is not necessarily integral; e.g., in Figs. 6(d) and 6(e) it equals $\Delta m = \Delta m' = 10$ and 5, respectively, although $\mu = \frac{10}{3}$ and $\frac{5}{2}$. If $\mu \equiv n/j$ is rational (with n and j relatively prime), the recurrence condition implies $\Delta m = \Delta m' = n$. There is therefore generally more than one type of pattern with the same period, such as $n = 10$ in Figs. 6(b) and 6(d) ($j = 1$ and 3) and $n = 5$ in Figs. 6(c) and 6(e) ($j = 1$ and 2). Even though slight variations in the value of μ include an excursion through irrational numbers, these may nevertheless be considered approximately rational in a well-defined sense (see Sec. V). Even the rational values $\mu = \frac{10}{3}$ in Fig. 6(d) and $\mu = \frac{5}{2}$ in Fig. 6(e) exhibit subdominant peaks at $\Delta m \approx \mu \approx 3$ and $\Delta m \approx \mu \approx 2$–3, respectively. However, this exposes a difficulty with applying this model directly to ramped fields in Rydberg atoms. In a linearly driven system the phase parameter varies with ramp rate as $\varphi \sim 1/\dot{F}$ [Eq. (10)], leading to the qualitative dependence of μ on $\dot{F}$ shown in Fig. 7. Variations in μ are therefore especially sensitive to $\dot{F}$ at slower ramps.

From Eq. (65) we also see that the repeated pattern of probabilities dilates and includes more oscillations either as d grows or as $|\varphi(\mathrm{mod} 2\pi)|$ decreases (i.e., as μ increases); see Figs. 5 and 6. This happens because the Bessel function makes excursions between $J_\nu(0)$ and $J_\nu(x_{\max})$ with a maximum argument $x_{\max} = \pm 2d/\sin(\pi/\mu)$. Furthermore, the small-x behavior of $J_\nu(x)$ [17] guarantees that appreciable population will be found only for intersections with

$$|m - m'| \lesssim 2d/\sin(\pi/\mu). \quad (69)$$
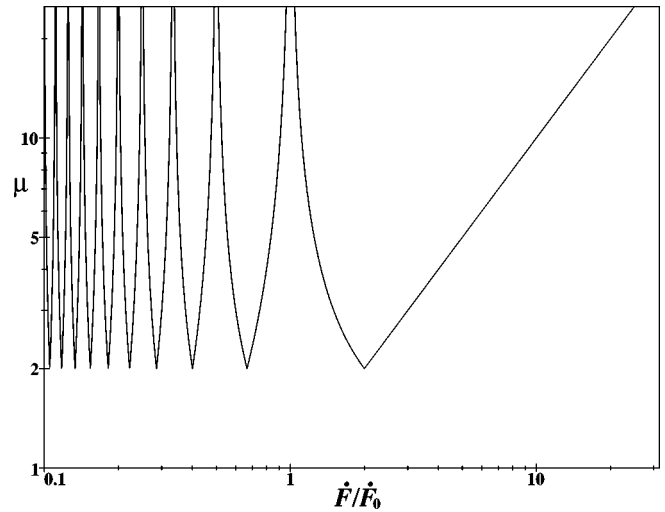
FIG. 7. A log-log plot of the level period μ [Eq. (66)] vs rescaled ramp rate $\dot{F}/\dot{F}_0$. Based on the dependence $\varphi \sim 1/\dot{F}$, this function is $\mu = 1/|(\dot{F}_0/\dot{F})(\mathrm{mod} 1)|$, where the modulus is taken between $-\frac{1}{2}$ and $+\frac{1}{2}$. A typical scale, from Eq. (10), is provided by $\dot{F}_0 \sim 1/6\pi n^{10}$ a.u. $= (40.3/n)^{10}$ kV/cm μs^{-1}.

This spread remains constrained even as m and m' increase, which should be contrasted with the undifferentiated hump of the PWeb model, whose width increases as $\sim d\sqrt{m + m'}$ (i.e., like a random walk) [18].

A degenerate case arises when $\varphi \rightarrow 0 (\mathrm{mod} 2\pi)$, shown in Figs. 4 and 6(a). Then $c_1(m', \varphi) \rightarrow m'$ and Eq. (65) assumes the noncyclic form

$$\mathcal{P}^{(\uparrow)}_{mm'}(d, \varphi) \xrightarrow[\mu \rightarrow \infty]{} |J_{|m' - m|}(2dm')|^2 \quad (70)$$

as long as $m' \leq \mu$. This result serves as a small-d approximation to the series form (61a) in Sec. III. Appreciable population can now be expected to be found [18] when $|m - m'| \lesssim 2dm'$ or

$$\frac{1}{1 + 2d} \lesssim \frac{m'}{m} \lesssim \frac{1}{1 - 2d}. \quad (71)$$

Both these bands were already seen in Figs. 4(b) and 4(c) and the upper one accords with Eq. (63) for small d.

In the opposite extreme of maximally destructive interference, when $\varphi(\mathrm{mod} 2\pi) \rightarrow \pm \pi$ and $\mu \rightarrow 2$, Eq. (69) implies a very narrow adiabatic band of surviving population. This case is plotted in Fig. 6(f). The sharp patterns seen in Figs. 6(a)–6(e) break up here, although there is a residue of a recurrence along a weaker band with $\Delta m = 2$. Resonances among the phases $\Sigma_{k=0}^{m'-1} \Theta(d; \theta' + k\varphi)$ in Eq. (52) quickly destabilize the amplitude in this case, as soon as $n > 1$ terms in Eq. (59) get magnified. In fact, the adiabatic pattern for any μ ultimately becomes unstable. If n is the smallest integer for which n/μ is approximately integral [i.e., $n\varphi \approx 0 (\mathrm{mod} 2\pi)$, $n \geq 2$], the term that is $\sim O(d^n)$ has $c_n(m', \varphi) \approx m'$ and is thus not bounded. The approximation (64) is then good only as long as at least this term can be ignored compared to the $n = 1$ term, implying

$$m' \lesssim \frac{n}{d^{n-1} \sin\left(\dfrac{\pi}{\mu}\right)} \qquad (72)$$

in general and $m' \lesssim 2/d$ for $\mu = 2$. Equation (72) serves to delimit the stability of the adiabatic result (65) since this m', representing duration, is always larger than the distribution width (69).

V. DIABATIC EVOLUTION

When the two-level transitions tend towards diabaticity $(D > A)$, terms of all orders d^n become significant in the expansion (56) of $\Theta(d; \vartheta)$. It is then appropriate to use instead of the phases (51) an expansion in powers of $1 - d$. Noting that the factors of Eq. (45) have the functional form $e^{i\beta}$ with $\beta = \pi - 2\tan^{-1}[\delta \cot(\frac{1}{2}\vartheta)]$ and $\vartheta = \theta' + (k+1)\varphi$, the diabatic analog of Eq. (59) is

$$\mathcal{A}_{mm'}^{(\uparrow)}(d,\varphi) = (-1)^{m'} e^{im\varphi} \frac{1}{2\pi} \int_0^{2\pi} d\theta'$$

$$\times \exp\left[-i\left\{ \sum_{n=1}^{\infty} \frac{2}{n} \delta^n b_n(m',\varphi;\theta') + m\theta' \right\} \right], \qquad (73)$$

with δ defined in Eq. (55). Here the sum runs over odd n only, while the sum over shifted phases gives

$$b_n(m',\varphi;\theta') = (-1)^{(n-1)/2} \sum_{k=0}^{m'-1} \cot^n(\tfrac{1}{2}\theta' + \tfrac{1}{2}k\varphi), \qquad (74)$$

in contrast to the closed form of Eq. (57) with its diffraction-like coefficient $c_n(m',\varphi)$. In the diabatic limit $(d \to 1)$, Eq. (55), we keep just the $n = 1$ term of Eq. (73):

$$\mathcal{A}_{mm'}^{(\uparrow)}(d,\varphi) = (-1)^{m'} e^{im\varphi} \frac{1}{2\pi} \int_0^{2\pi} d\theta'$$

$$\times \exp\left[-i\left\{ 2\delta \sum_{k=0}^{m'-1} \cot(\tfrac{1}{2}\theta' + \tfrac{1}{2}k\varphi) \right.\right.$$

$$\left.\left. + \cdots + m\theta' \right\} \right]. \qquad (75)$$

For the perfectly diabatic case $(\delta = 0)$, this reduces to Eq. (38a). Otherwise, Eq. (75) cannot be handled straightforwardly on account of the uneven distribution of poles in the sum of cotangents.

Figure 8 shows the exact up- and down-going probabilities for $\varphi = \frac{1}{4}\pi$ and for three values of d approaching unity. The populations $\mathcal{P}_{mm'}^{(\uparrow)}(d,\varphi)$ become markedly asymmetric, peaking preferentially along loci of levels nearly parallel to one another and to the original $m = 0$ level, thereby forming "resonance lanes" on the grid. These diabatic results are to be contrasted with the more adiabatic cases shown in Figs. 5 and 6, where high probability is associated with proximity to the purely adiabatic path $(m' \approx m)$. This new diabatic type

of time-evolution pattern in fact arises as a modified form of the adiabatic braids seen in Fig. 5: one of the arms that passes through each recurrence peak (68) can be described as undergoing a rotation on the grid, while the other arm fades away. (Both branches of the down-going populations fade as $d \to 1$.) The degree of this rotation is given by the same formula, Eq. (63), that characterizes the evolutionary path for the $\varphi = 0$ case.

The resonances in $\mathcal{P}_{mm'}^{(\uparrow)}(d,\varphi)$ in Figs. 8(b) and 8(c) are concentrated along up-going levels whose indices m are integral multiples of the period $\mu = 8$ [Eq. (66)]. Accompanying the exponential decay of the $m = 0$ state population with increasing m' is the growth of the parallel $m = 8$ level, which in turn transfers population to $m = 16$, etc. In general, evolutionary paths whose dynamical phases differ by $0 \pmod{2\pi}$ will interfere constructively. Since the unit of phase [Eq. (8)] is $\varphi = \frac{1}{8}(2\pi)$ here, the phase difference (7) should encompass 0, 8, 16, ... such units. Moreover, to maximize probability when a is small, loss from state-to-state diffusion should be minimized, which favors paths with few adiabatic transitions (e.g., two). The initial evolution, which follows the purely diabatic path, has many branches to $m = 8$ that satisfy these conditions and thus favors strong resonances between states having $m = 0$ and 8. Likewise, the increased $m = 8$ population resonates strongly with $m = 16$ and so forth, forming the up-going lanes seen in the figure. No such optimization can occur for constant-m' paths, so down-going levels are relatively insignificant in the diabatic limit. That is, there is a kind of "diabatic momentum" to the evolution of interacting manifolds.

In the special case $\varphi = 0 \pmod{2\pi}$ all dynamical phases vanish; then Eq. (75) simplifies to

$$\mathcal{A}_{mm'}^{(\uparrow)}(d,0) = (-1)^{m'} \frac{1}{2\pi} \int_0^{2\pi} d\theta'$$

$$\times \exp[-i\{2\delta m' \cot(\tfrac{1}{2}\theta') + m\theta'\}]. \qquad (76)$$

Substitution of $z = \cot(\frac{1}{2}\theta')$ yields

$$\mathcal{A}_{mm'}^{(\uparrow)}(d,0) = (-1)^{m'} \frac{1}{\pi} \int_{-\infty}^{\infty} dz \, e^{-i(2\delta m')z} \frac{(z-i)^{m-1}}{(z+i)^{m+1}}, \qquad (77)$$

which is recognized as the integral representation of a Whittaker function [19]. In the diabatic limit, therefore, the populations

$$\mathcal{P}_{mm'}^{(\uparrow)}(d,0) = |(4\delta m') e^{-2\delta m'} {}_1F_1(-(m-1);2;4\delta m')|^2 \qquad (78)$$

are seen to vary like the probability density of a squared Coulomb function (for $Z = 1$) evaluated at a "radius" $r = 2\delta mm'$ and having effective quantum numbers $n_{\text{eff}} = m$ and $l_{\text{eff}} = 0$.

A scaling relation for $d \to 1$ follows for nonintegral but rational $\mu \equiv n/j$ based on the above limiting integrals. When $m = Mn$ and $m' = M'n$ are both integral multiples of the integer n $(M, M' \geqslant 0)$, the sum of cotangents in Eq. (75)
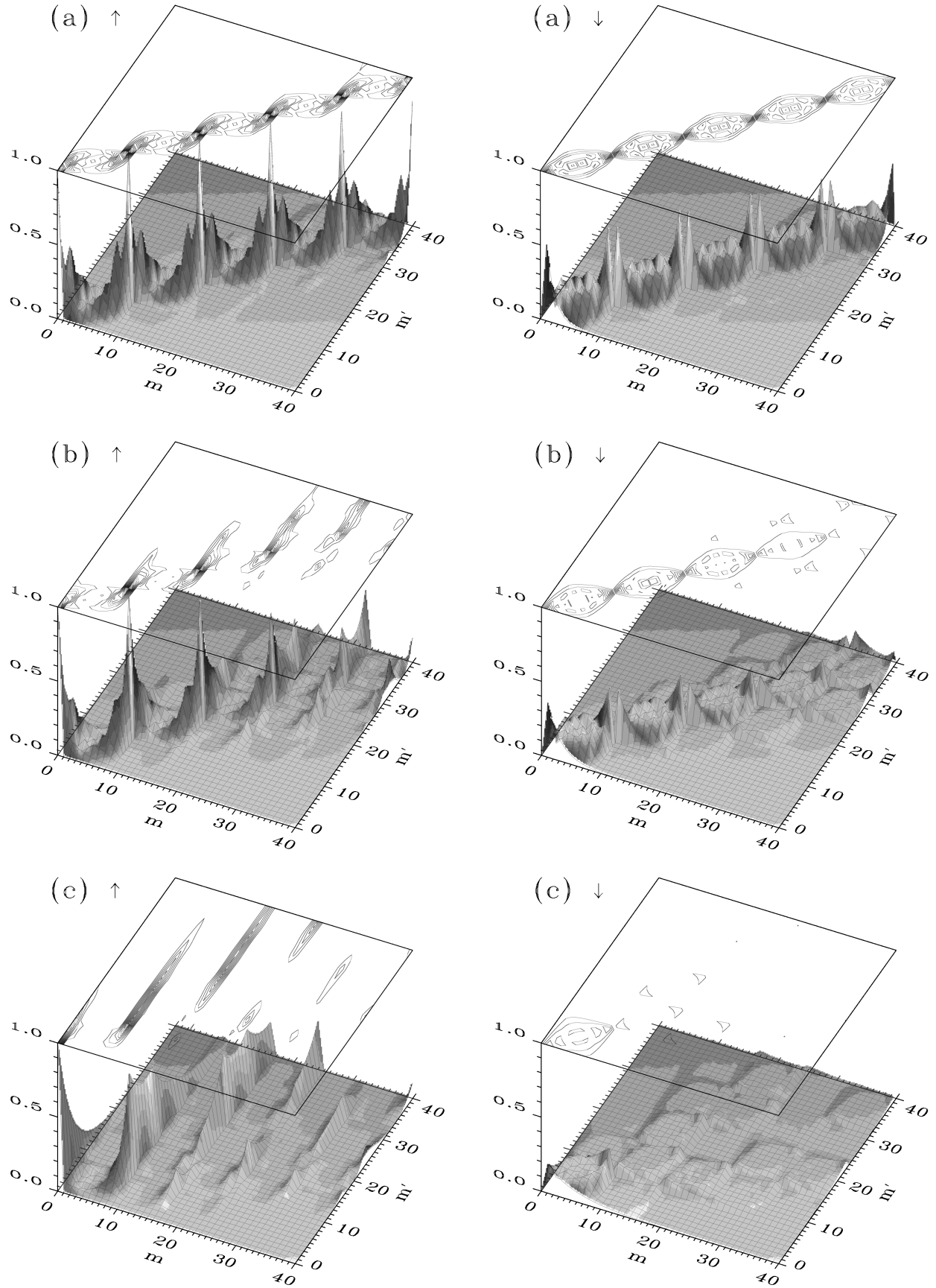
FIG. 8. Three-dimensional and contour plots of probabilities $\mathcal{P}_{mm'}^{(\uparrow)}(d,\varphi)$ (left) and $\mathcal{P}_{mm'}^{(\downarrow)}(d,\varphi)$ (right) vs (m,m') in the diabatic approximation [cf. Eq. (78)] for fixed $\varphi=\frac{1}{4}\pi$ ($\mu=8$) and larger values of $D=d^2\to1$: (a) $d=0.70$, (b) 0.80, and (c) 0.90. Contours are as in Fig. 4.

reduces to $M'n \cot(n\theta')$. Then a redefinition of the variable to $\theta'' = n\theta'$ yields an integral of the form of Eq. (76), which implies

$$\mathcal{P}_{Mn,M'n}^{(\uparrow)}\left(d, \frac{2\pi j}{n}\right) = \mathcal{P}_{M,M'n}^{(\uparrow)}(d,0). \qquad (79)$$

Thus, for $\varphi = 2\pi j/n$, up-going-level populations are still given by the analytical result (78) for $\varphi(\mathrm{mod}\,2\pi) = 0$, at least near the intersections $[Mn,M'n]$, except for an inflation by a factor of n along the m axis. Note, however, that a comparison of this rescaling with a numerical calculation of $\mathcal{P}_{mm'}^{(\uparrow)}(d,\varphi)$ has found it to hold accurately only in the extreme diabatic limit (e.g., $d > 0.9$).

When μ is nonintegral or even irrational, one can still observe quasirevivals in the time evolution. Figure 9 shows $\mathcal{P}_{mm'}^{(\uparrow)}(d,\varphi)$ for a very diabatic case and three slightly different values of the number of phase cycles per unit of action $\alpha \equiv 1/\mu = \varphi/2\pi \approx \frac{3}{8}$. As expected, the rational case [Fig. 9(a)], with numerator $j = 3$ and denominator $n = 8$, displays prominent resonances along $m = 8, 16, 24,$ and 32, as well as smaller peaks along constant-m lanes approximately one-

third of the way between the main lanes. The latter resonances are made plausible by a continued-fraction expansion of α for this case:

$$\frac{3}{8} = \cfrac{1}{2 + \cfrac{1}{1 + \cfrac{1}{2}}} \approx \frac{1}{2} \rightarrow \frac{1}{3} \rightarrow \frac{3}{8}, \qquad (80a)$$

where the chain of "convergents," which follow from keeping successive denominators of the expansion, represent ever better approximations to the actual value of α [20]. On the basis of these estimates of j/n, resonances are expected at spacings of $\Delta m = n = 2, 3,$ and 8. With the assumption that improved values produce more substantial peaks, the appearance of subsidiary resonances for rational but nonintegral values of $\alpha = 1/\mu$ is predictable.

Turning to the irrational cases in Figs. 9(b) and 9(c), we see that the evolution in these cases is similar to Fig. 9(a) up to the first main lane at $m = 8$ and thereafter less and less similar, the more so for Fig. 9(c), whose value for α departs further from $\frac{3}{8}$. For Figs. 9(b) and 9(c) we have the continued fractions

$$\frac{1}{\sqrt{7}} = \cfrac{1}{2 + \cfrac{1}{1 + \cfrac{1}{1 + \cfrac{1}{1 + \cfrac{1}{4 + \cfrac{1}{1 + \ddots}}}}}} \approx \frac{1}{2} \rightarrow \frac{1}{3} \rightarrow \frac{2}{5} \rightarrow \frac{3}{8} \rightarrow \frac{14}{37} \rightarrow \frac{17}{45} \rightarrow \cdots \qquad (80b)$$

and

$$\frac{3 - \sqrt{5}}{2} = \cfrac{1}{2 + \cfrac{1}{1 + \cfrac{1}{1 + \cfrac{1}{1 + \cfrac{1}{1 + \ddots}}}}} \approx \frac{1}{2} \rightarrow \frac{1}{3} \rightarrow \frac{2}{5} \rightarrow \frac{3}{8} \rightarrow \frac{5}{13} \rightarrow \frac{13}{21} \rightarrow \cdots . \qquad (80c)$$

Although the correspondence is not perfect, we see in Fig. 9(b) the expected peaks along $m = n = 2, 3, 5, 8$ and some of their multiples given in Eq. (80b). The especially large peak at $m = 37$ may be ascribed to a more substantial correction to a convergent coming from a large denominator of the continued fraction (4 in this case), which supports the above assumption regarding peak heights. (The extra peak along $m = 29$ follows from approximating the fifth convergent by replacing the denominator 4 with $3 + \frac{1}{1}$, producing the intermediate fraction $\frac{11}{29}$.) The fraction (80c) is related to the golden mean, so its expansion produces the Fibonacci series of integers. The peaks seen along $m = 3, 5, 8, 13, 21,$ and 34 (and their multiples) indeed correspond to the denominators n from this series.

The use of continued-fraction convergents should also apply in the adiabatic limit. Though the arguments presented

here rationalize the appearance of resonance peaks in the time evolution on a LZ grid, the association of their relative heights with particular convergents awaits quantitative prediction.

VI. CONCLUSION

The AWeb model considered here exhibits two general classes of coherent time evolution, roughly adiabatic and diabatic. When the two-level interactions are governed by adiabatic transitions, the redistribution of probability from a single initial state follows a pattern that recurs in time in the neighborhood of the purely adiabatic path. Then only those states tend to be populated whose levels lie near the center of the manifold-mixing region. When, on the other hand, the two-level transitions are predominantly diabatic, appreciable
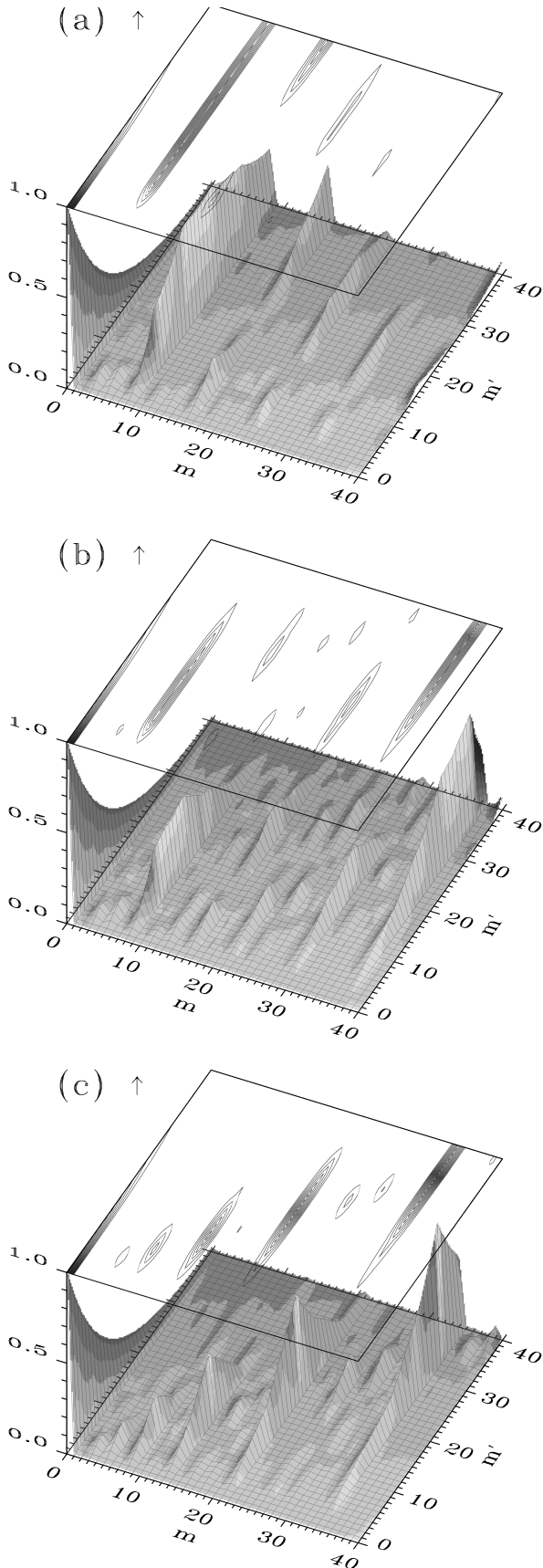
FIG. 9. Three-dimensional and contour plots of probabilities $\mathcal{P}^{(\uparrow)}_{mm'}(d,\varphi)$ vs (m,m') in the diabatic approximation [cf. Eq. (75)] for fixed $d=0.95$ and nearly equal $\alpha=(\varphi/2\pi)(\mathrm{mod}\,1)$: (a) $\alpha=\frac{3}{8}=0.375\,00$, (b) $\alpha=1/\sqrt{7}=0.377\,96...$, and (c) $\alpha=(3-\sqrt{5})/2=0.381\,96...$. Contours are as in Fig. 4.

probability is found only along lanes of certain up-going levels. These levels are parallel to the initial one and have quasiregular spacings that depend sensitively on the unit of phase φ. One might also distinguish the more sharply peaked constructive interference patterns for $\varphi(\mathrm{mod}\,2\pi)=0$, which are to be found for any transition probability D, but these may be viewed as special cases of the adiabatic and diabatic distributions.

It is interesting that many similar models that involve sets of interacting levels undergoing forces linear in t display the same partitioning of a state's time evolution into two types of distributions: a sharp diabatic one prevalent at relatively fast ramps and an adiabatic one, possibly more diffuse and involving more complex structure, at slow ramps. The two-level LZ model itself [3] is of course the prototypical system. In the Demkov-Osherov model [5], one level passes through and interacts with a manifold of parallel levels; the interloper exponentially decays and diffuses into the manifold. We have generalized this here in the AWeb model to the pairwise interaction of levels from two whole manifolds. The extension of one up-going interloper (Demkov-Osherov) to a set of coherently evolving up-going levels (AWeb) accordingly extends the decay of that one level to the resonant population and decay of a set of levels parallel to an initially populated one. The PWeb model [6], the incoherent version of the Aweb model, also finds a sharp distribution in the extreme diabatic limit, but otherwise there is a single, diffuse bump in the mixing region of the grid.

A subtle point is that the incoherent probability distributions for the PWeb model at given N (see the Appendix) do *not* generally follow from the coherent AWeb model by simply averaging $\mathcal{P}^{(\uparrow)}_{mm'}(d,\varphi)$ or $\mathcal{P}^{(\downarrow)}_{mm'}(d,\varphi)$ over φ after traversal of a fixed number N of avoided crossings [21]. A measurement that destroys an interference pattern *after* the system has already evolved coherently will not necessarily reproduce the pattern arising from evolution that has been incoherent throughout.

This general twofold behavior of the patterns of evolution has also been observed in investigations of Stark states and SFI of Rydberg atoms [8]. The ''bowtie'' model [4] of state mixing among *nonparallel* levels of a single Rydberg n-manifold identifies a high probability of only diabatic or adiabatic transitions, in the context of a multilevel generalization of the two-level LZ effect. Most generally, for low m_l, high enough n, and fast enough ramp rates, one expects to see a sharp diabatic signal from a succession of diabatic transitions, whereas at lower n or $\dot{F}$, in most cases one sees a more diffuse adiabatic signal, possibly with some structure, from mostly adiabatic transitions among Rydberg manifolds. A precise analysis of SFI is complicated by several issues: Each manifold's levels are not parallel; the couplings, and hence the values of D, φ, and Φ_S, vary from one anticrossing to the next; the avoided crossings might be so broad as to be not even distinct (as in Na); and in the region of a Stark map below the classical ionization limit, for given n, not 2 but at least $3n/16$ manifolds will cross and mix. The greatest difficulty in grafting simple models onto realistic atomic problems stems from the extreme sensitivity of any interference to the dynamical phases, especially in the adiabatic limit, and the rapidly increasing accumulation of phase at

higher fields as nonparallel Stark levels diverge.

In a recent theoretical study of Stark maps [22] and SFI in Rydberg atoms, direct numerical integration of the Schrödinger equation, including couplings among all levels, produced field-ionization populations that qualitatively mimic the diabatic and adiabatic signals observed in SFI experiments [23]. These calculations advanced a cruder study [24] of SFI that considered only two-level couplings but also produced reasonable quasi-ionization signals at a qualitative level. More accurate calculations are planned and are needed to understand how models such as the AWeb can be applied to the interpretation of experiments on coherent-state mixing.

Note added in proof. Experimental evidence of quantum resonances, recurrences, and suppression of diffusion on a Landau-Zener grid realized in a classical optical system (an ''optical Galton board'') has been obtained by Dirk Bouwmeester, Ph.D. thesis, University of Leiden, 1995 (unpublished). Steven van Enk (private communication).

APPENDIX

The incoherent PWeb model of Ref. [6] requires no phase information and so depends only on the diabatic transition probability D. Generating functions for up- and down-going probabilities are obtained by following the steps detailed in Sec. II, Eqs. (24)–(29), with the following changes: (i) the operators $\hat{\tilde{\xi}}$ and $\hat{\eta}$ commute (effectively, $\varphi = 0$) and so are just dummy variables [13]; (ii) the 2×2 amplitude-mixing matrix $\begin{pmatrix} -d & a \\ a & d \end{pmatrix}$ in Eqs. (25) and (27) must be replaced by the probability-mixing matrix $\begin{pmatrix} D & A \\ A & D \end{pmatrix}$ where $A \equiv 1 - D$; and (iii) the amplitudes $\mathcal{A}_{mm'}^{(\uparrow)}(d,\varphi)$ and $\mathcal{A}_{mm'}^{(\downarrow)}(d,\varphi)$ should be replaced with probabilities $\mathcal{P}_{mm'}^{(\uparrow)}(D)$ and $\mathcal{P}_{mm'}^{(\downarrow)}(D)$ in all formulas. In analogy to Eqs. (24a) and (24b) we define the generating functions

$$\mathcal{P}^{(\uparrow)}(D) \equiv \sum_{m=0}^{\infty} \sum_{m'=0}^{\infty} \mathcal{P}_{mm'}^{(\uparrow)}(D)\xi^m \eta^{m'}, \qquad \text{(A1a)}$$

$$\mathcal{P}^{(\downarrow)}(D) \equiv \sum_{m=0}^{\infty} \sum_{m'=0}^{\infty} \mathcal{P}_{mm'}^{(\downarrow)}(D)\xi^m \eta^{m'}. \qquad \text{(A1b)}$$

These functions satisfy the 2×2 matrix equation

$$\begin{pmatrix} \mathcal{P}^{(\uparrow)}(D) \\ \mathcal{P}^{(\downarrow)}(D) \end{pmatrix} = \begin{pmatrix} 1 \\ 0 \end{pmatrix} + \begin{pmatrix} \eta & 0 \\ 0 & \xi \end{pmatrix}\begin{pmatrix} D & A \\ A & D \end{pmatrix}\begin{pmatrix} \mathcal{P}^{(\uparrow)}(D) \\ \mathcal{P}^{(\downarrow)}(D) \end{pmatrix}, \quad \text{(A2)}$$

whose solution is

$$\mathcal{P}^{(\uparrow)}(D) = \frac{1 - D\xi}{1 - D(\xi + \eta) + (D - A)\xi\eta}, \qquad \text{(A3a)}$$

$$\mathcal{P}^{(\downarrow)}(D) = \frac{A\xi}{1 - D(\xi + \eta) + (D - A)\xi\eta}. \qquad \text{(A3b)}$$

Expansion of these functions in powers of ξ and η and identification of their coefficients with the probabilities in Eqs. (A1a) and (A1b) lead to all the PWeb results found in Ref. [6].

[1] *Rydberg States of Atoms and Molecules*, edited by R. F. Stebbings and F. B. Dunning (Cambridge University Press, New York, 1983).

[2] T. F. Gallagher, *Rydberg Atoms* (Cambridge University Press, New York, 1994).

[3] C. Zener, Proc. R. Soc. London, Ser. A **137**, 696 (1932).

[4] D. A. Harmin, Phys. Rev. A **44**, 433 (1991).

[5] Yu. N. Demkov and V. I. Osherov, Zh. Eksp. Teor. Fiz. **53**, 1589 (1967) [Sov. Phys. JETP **26**, 916 (1968)].

[6] D. A. Harmin and P. N. Price, Phys. Rev. A **49**, 1933 (1994).

[7] V. N. Ostrovsky, in *Abstracts of the Eighth International Conference on the Physics of Electronic and Atomic Collisions, Belgrade, 1973*, edited by B. C. Čobić and M. V. Kurepa (Institute of Physics, Belgrade, 1973), p. 133; Yu. N. Demkov and V. N. Ostrovsky, J. Phys. B **28**, 403 (1995); Yu. N. Demkov, P. B. Kurasov, and V. N. Ostrovsky, J. Phys. A **28**, 4361 (1995).

[8] SFI is a widely used technique for atomic state diagnosis. See, e.g., (a) Ref. [1], Chaps. 3 and 9; (b) Jeys *et al.*, Phys. Rev. Lett. **44**, 390 (1980); (c) K. B. MacAdam, L. G. Gray, and R. G. Rolfes, Phys. Rev. A **42**, 5269 (1990); (d) Ref. [2], Chap. 7, and references therein.

[9] K. Mullen, E. Ben-Jacob, Y. Gefen, and Z. Schuss, Phys. Rev. Lett. **62**, 2543 (1989).

[10] Variation of the Stokes phase Φ_S from one intersection to the next (''disorder'') can have important effects. In a system similar to the present model, disorder in one-dimensional crystals driven by a linear magnetic flux produces additional localization in energy of the evolving state. D. Lubin, Y. Gefen, and I. Goldhirsch, Phys. Rev. B **41**, 4441 (1990).

[11] The term ''dynamical phase'' is used here in contradistinction to the topological ''adiabatic phase'' introduced by M. V. Berry, Proc. R. Soc. London, Ser. A **392**, 45 (1984).

[12] The result of Eq. (8) for the area of the parallelograms that tessellate the map of diabatic levels (1) shown in Fig. 1 can be derived using simple geometry. The vertical spacings ε and ε' and slopes p and $p' \neq p$ of each manifold's levels are arbitrary. An exotic but obvious extension would be to any grid of levels $\{E_m(t)\}$ and $\{E_{m'}(t)\}$ that tessellate the E-t plane; the phase φ would still be given by the area of each ''tile.''

[13] The expansion parameters ξ and η here play the respective roles that x^{-1} and x played in Sec. V of Ref. [6].

[14] Allowing for $D = d^2$, the absolute square of Eq. (34) reproduces Eq. (18) of Ref. [6].

[15] The statistical arguments leading to the PWeb up-going probabilities $P_{mm',\uparrow}^{(N)}(D)$, Eq. (16) and Ref. [18] of Ref. [6], identify paths with k pairs of adiabatic transitions and a total of

$m+m'-2k$ diabatic ones, of which $m'-k$ are of the up-to-up variety, for a path probability of $A^{2k}D^{N-2k}$. The amplitude factors of the present Eq. (61) therefore partition themselves as $a^{2k}(-d)^{m'-k}d^{m-k}$ [$m'-k\equiv u_k$ in Eqs. (11) and (12)], with the multiplicity of each such type of path the same in both models. Here, of course, one must square the series.

[16] Yet another form for the series (61a), good for $m>0$ and $m'>0$, is

$$\mathcal{A}_{mm'}^{(\uparrow)}(d,0)=a^2 d^{m-m'}\sum_{k=0}^{m'-1}\binom{m+k}{m}\binom{m-1}{m'-1-k}(-d^2)^k.$$

[17] The population is not considered ''appreciable'' here unless $|x_{\max}|>j'_{\nu,1}$, where $j'_{\nu,1}$ marks the first maximum of the Bessel function of order $\nu>1$. According to M. Abramowitz and I. A. Stegun, *Handbook of Mathematical Functions* (Dover, New York, 1970), Sec. 9.5, dJ_ν/dx has zeros at $j'_{\nu,1}\approx\nu+0.82\nu^{1/3}$, so Eq. (69) slightly overestimates ν and Eq. (71) underestimates the spread of the slopes m'/m.

[18] Equation (34) of Ref. [6] gives the half-width of the hump in the adiabatic limit as $|m-m'|\lesssim DN$. The absence of interference in the PWeb model allows diffusion of population away from the adiabatic path to take place.

[19] M. Abramowitz and I. A. Stegun, *Handbook of Mathematical Functions* (Ref. [17]), Chaps. 13 and 14.

[20] M. Abramowitz and I. A. Stegun, *Handbook of Mathematical Functions* (Ref. [17]), Sec. 3.10.

[21] Note that the generation number N [Eq. (16)] is not proportional to t for an asymmetric grid. The ''forced decoherence'' of the AWeb does in fact reproduce PWeb probability distributions, but only up to $N=6$.

[22] M. L. Zimmerman, M. G. Littman, M. M. Kash, and D. Kleppner, Phys. Rev. A **20**, 2251 (1979); see also T. F. Gallagher, *Rydberg Atoms* (Ref. [2]), Chap. 6.

[23] Timothy R. Symons, M. S. thesis, University of Kentucky, 1997 (unpublished).

[24] D. A. Harmin (unpublished).